Refinement of the environmental and chronological context of the archeological site El Harhoura 2 (Rabat, Morocco) using paleoclimatic simulations.

Léa Terray[1], Emmanuelle Stoetzel[2], Eslem Ben Arous[3,4,2], Masa Kageyama[5], Raphaël Cornette[1] and Pascale Braconnot[5]

[1] Institut de Systématique, Evolution, Biodiversité (ISYEB) – UMR 7205, Muséum National d'Histoire Naturelle, CNRS, Sorbonne Université, EPHE, Université des Antilles, Paris, France.

[2] Histoire Naturelle de l'Homme Préhistorique (HNHP) – UMR 7194, CNRS, Muséum National d'Histoire Naturelle, Sorbonne Université, UPVD, Musée de l'Homme, Paris, France.

[3] Pan-African Evolution Research Group (Pan-Ev), Max Planck Institute for the Science of Human History, Jena, Germany.

[4] Geochronology lab, Centro Nacional de Investigación sobre la Evolución Humana, Burgos, Spain

[5] Laboratoire des Sciences du Climat et de l'Environnement (LSCE) – UMR 8212 / Institut Pierre Simon Laplace (IPSL) – UMR 8112, CEA/CNRS/UVSQ, Centre CEA-Saclay, Gif-sur-Yvette, France

Correspondence to: Léa Terray (lea.terray@gmail.com)

Abstract.

This study illustrates the strong potential of combining paleoenvironmental reconstructions and paleoclimate modeling to refine the paleoenvironmental and chronological context of archaeological and paleontological sites. We focus on the El Harhoura 2 cave (EH), an archeological site located on the North-Atlantic coast of Morocco that covers a period from the Late Pleistocene to the mid-Holocene. On several stratigraphic layers, inconsistencies are observed between species presence and isotope-based inferences used to reconstruct paleoenvironmental conditions. The stratigraphy of EH also shows chronological inconsistencies on older layers between age estimated by Optical Stimulated Luminescence (OSL) and Combination of Uranium Series and Electron Spin Resonance methods (combined US-ESR). To infer global paleoclimate variations over the EH sequence in the area, we produced an ensemble of atmosphere-only simulations using the LMDZOR6A model, using boundary conditions and forcings from pre-existing coupled simulations to match the different key periods. We conducted a consistency approach between paleoclimatic simulations and paleoenvironmental inferences available from EH. Our main conclusion show that the climate sequence based on combined US-ESR ages is more consistent with paleoenvironmental inferences than the climate sequence based on OSL ages. We also evidence that isotope-based inferences are more consistent with the paleoclimate sequence than species-based inferences. These results highlight the difference in scale between the information provided by each of these paleoenvironmental proxies. Our approach is transferable to other sites due to the increase number of available paleoclimate simulations.

1 Introduction

The reconstruction of paleoenvironments has long been a subject of great interest, particularly to study the past biodiversity. Archeological sites provide unique opportunities to infer paleoenvironements from faunal and/or vegetal remains (e.g., Avery, 2007; Denys et al., 2018; Stoetzel et al., 2011; Comay and Dayan, 2018; Matthews, 2000; Marquer et al., 2022) or stable light isotope composition of sediments or biological remains (e.g. Tieszen, 1991; Royer et al., 2013). These approaches allow one to characterize the past landscapes and biotic environments in the vicinity of the sites. Inconsistencies between isotopic compositions, differences in type of remains, and variations in stratigraphies are often to be faced and and prevent proper assessment of the possible relationships between biodiversity and paleoenvironmental changes.

This is the case for the El Harhoura 2 (EH) cave, an archeological site located on the North-Atlantic coast of Morocco, that we use here as a case study. At EH, paleoenvironments have mainly been inferred based on two different kinds of proxies: species presence and stable light isotope composition. Because of species habitat preferences, the presence and/or abundance of particular taxa is a strong indicator of certain types of environment, such as amphibians for more humid contexts, or gerbils and jerboas for more arid contexts (e.g., Fernandez-Jalvo *et al.*, 1998; Stoetzel *et al.*, 2011). Stable light isotope composition of teeth of small mammals provide varied indications about diet and paleoenvironments (Longinelli and Selmo, 2003; Navarro et al., 2004; Royer et al., 2013), and thus about aridity, seasonal variations of climate and vegetal cover. At EH, inconsistencies are observed between species presence and isotope-based inferences (Jeffrey, 2016; Stoetzel et al., 2019). On two stratigraphic layers (over eight well studied layers), while species presence suggests drier conditions than usual, isotopic composition of Meriones teeth suggest a more humid and temperate climate. Such discrepancies are not fundamentally surprising, because species presence and isotopic composition do not deliver the exact same information: species presence carries a signal at the scale of faunal communities, while isotopic composition reflects the diet preferences of a limited number of individuals of a single species. But these mixed messages make it difficult to extrapolate the environmental conditions of the site.

The stratigraphy of EH also shows some chronological inconsistencies. Radiocarbon dating (AMS-^{14}C) is the most reliable dating method, however it cannot date remains older than 50 ka. Beyond this reach, other dating methods must be applied, such as Optical Stimulated Luminescence (OSL) and Combination of Uranium Series and Electron Spin Resonance methods (combined US-ESR). It has been shown that OSL and combined US-ESR methods display important differences in the estimated age of the same stratigraphic layers (Ben Arous et al., 2020b). These differences are related to the fact that these dating methods do not date the same objects. OSL estimates the last time quartz sediment was exposed to light, while combined US-ESR estimates the age of fossil teeth. To date, the respective reliability of these methods is difficult to establish.

These kind of paleoenvironmental and chronological discrepancies are widespread in archeology and paleontology. Climate-model simulations may inform us about the broader climate influences over the region, and therefore might enrich our understanding of the large-scale climate changes. Climate models simulate paleoclimates using the physical laws that describe the dynamics and thermodynamics of the Earth system, and model-data comparisons have shown that the large scale patterns are consistent with paleoclimatic simulations, even though regional feature are underestimated or affected by model biases (Kutzbach and Otto-Bliesner, 1982; Braconnot et al., 2012; Duplessy and Ramstein, 2013; Schmidt et al., 2014; Harrison et al., 2015). They thus offer a consistent framework for testing the consistency between climate drivers and environmental changes recorded at EH.

In this paper, we use coupled simulations performed over the past ten years with the IPSL model to derive an ensemble of atmosphere-only simulations, using boundary conditions and forcings from the coupled simulations to match different key periods in the past, with the latest version of the model (Boucher et al., 2020; Hourdin et al., 2020). This version is chosen because it of its skill in reproducing the climate in the region. However, because of the differences in scale and resolution between the archaeological record and the paleoclimate simulations, several caveats must be considered beforehand. Firstly, archaeological and paleoclimate data present different temporal resolution. Paleoclimate simulations present snapshots of the climate state consistent with the boundary conditions specified for a particular time. Conversely, an archeological layer is a stratigraphic/sedimentary unit that can cover shorter or longer periods and undergoes microclimatic variations that cannot be disentangled. Nevertheless, because EH is dated from the Late Pleistocene to the mid-Holocene period (Marine Isotopic Stages (MIS) 5 to 1), which in the area is marked by important global climatic fluctuations over time (i.e. the last glacial-interglacial transition; e.g., Hooghiemstra *et al.*, 1992; deMenocal, 1995, 2004; Le Houérou, 1997; Carto *et al.*, 2009; Trauth *et al.*, 2009; Drake *et al.*, 2011, 2013; Blome *et al.*, 2012; Kageyama *et al.*, 2013; Couvreur *et al.*, 2020), we do not expect these differences in temporal scale and resolution between the archaeological record and the paleoclimate simulations to prevent a global consistency approach. Secondly, archaeological and paleoclimate data present different spatial resolution. The spatial resolution of the atmospheric grid use here is ~150 km (Boucher et al., 2020). Conversely, EH represents a precise locality, and most species whose presence was recorded have a lifetime dispersal range largely inferior to 150 km (e.g., the jird *Meriones shawii* has a home range estimated between 200-1000 m^2 (Ghawar et al., 2015)). Then, the climate described by the global simulations cannot faithfully represent microclimate variations at EH. We make the assumption that the results of the global climate simulations are sufficient to capture the large climate changes we are interested in. Regional dynamical or statistical approaches would be derived from these simulations and could add additional unknowns due to the fact that the tuning of these methods has to be done using present day observations at the site. The cave is now imbedded in an urban area that experiences rapid climate and environmental changes over the last century and it is unclear that tuning over this recent period would be valid for the past conditions we are considering in this study.

In order to discuss and refine the paleoenvironmental and chronological context of EH, we conduct a consistency approach between paleoclimate simulations and paleoenvironmental inferences based on EH content from the literature. To overcome the issue of the differences between dates estimated with different methods, we considered two separate chronological sequences based on different dating method. Finally, for each of the chronological sequences, we examine the consistency between paleoclimate variables extracted from simulations, and species presence and stable light isotope composition. We expect this consistency approach to discriminate paleoenvironmental inconsistencies between species- and isotope-based proxies, and also eventually to distinguish between the two chronological sequences, and therefore between the two dating methods.

The remainder of the manuscript is organized as follows. We present the EH cave and the different choices made to run the set of paleoclimatic simulations in section 2. In section 3 we present the consistency analyses and the results. The discussion in section 4 highlights the major results and the proof of concept of the proposed approach, before the general conclusion (section 5).

2 Material and methods

2.1 El Harhoura 2 cave

2.1.1 Presentation of the site

The archeological site EH is located on the Moroccan Atlantic coast in the Rabat-Témara region (33°57’08.9” N / 6°55’32.5” W). The climate of the area is marked by a strong seasonal variability (**Fig 1**) with a relatively warm and dry summer during which precipitation is almost absent and evaporation is particularly high, and a relatively cool and short winter, which is also the rainy season (Sobrino and Raissouni, 2000; Lionello et al., 2006). Inferences based on species presence and abundances suggest that, in the past, the site underwent important climatic fluctuations, which resulted in a succession of relatively humid/arid and open/closed environments at EH (Stoetzel, 2009; Stoetzel et al., 2011, 2012a, b). As a result, paleolandscapes of the Late Pleistocene are described as open steppe or savanna-like lands with patches of shrubs, woodlands and water bodies, the latter expanding during wet periods, especially during the mid-Holocene (Stoetzel, 2009; Stoetzel et al., 2012a, 2014).

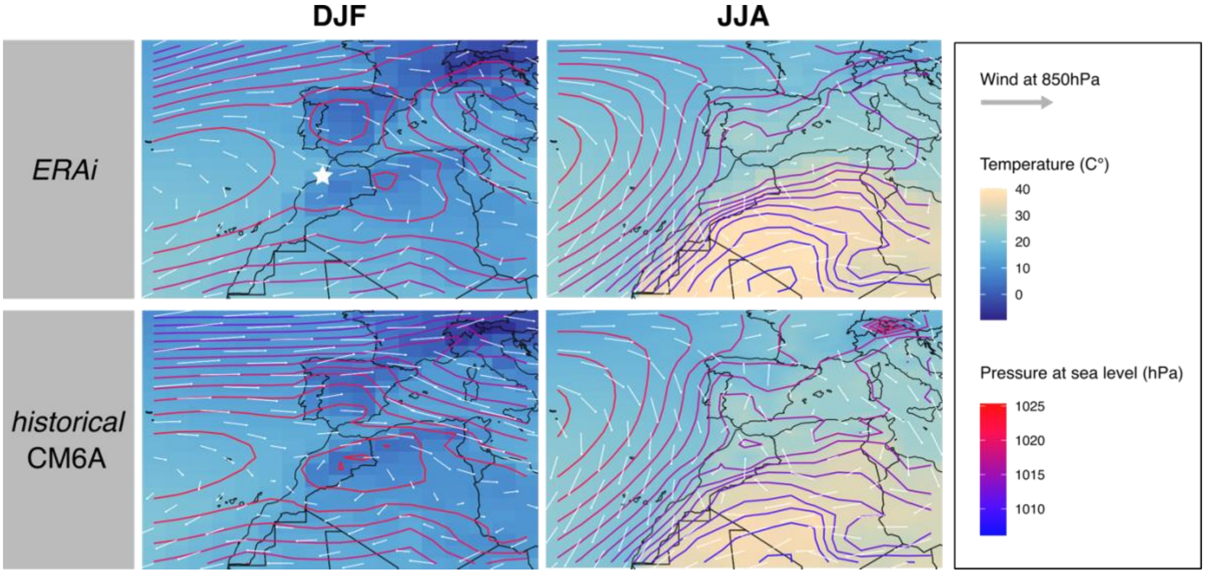

Fig. 1. Maps of mean temperature (unit: °C), wind speed and direction at 850hPa (represented by arrows, length is proportional to wind speed) and corrected pressure at sea level (unit: hPa) per season of the global atmospheric reanalysis ERA-interim (ERAi; Berrisford et al., 2011) and the *historical* simulations of IPSL-CM6-LR models on the region of EH. Data were averaged on 30 seasonal cycles (1980-2009). EH cave location is represented by a star in the upper left panel. DJF: December, January, February (winter); JJA: June, July, August (summer).

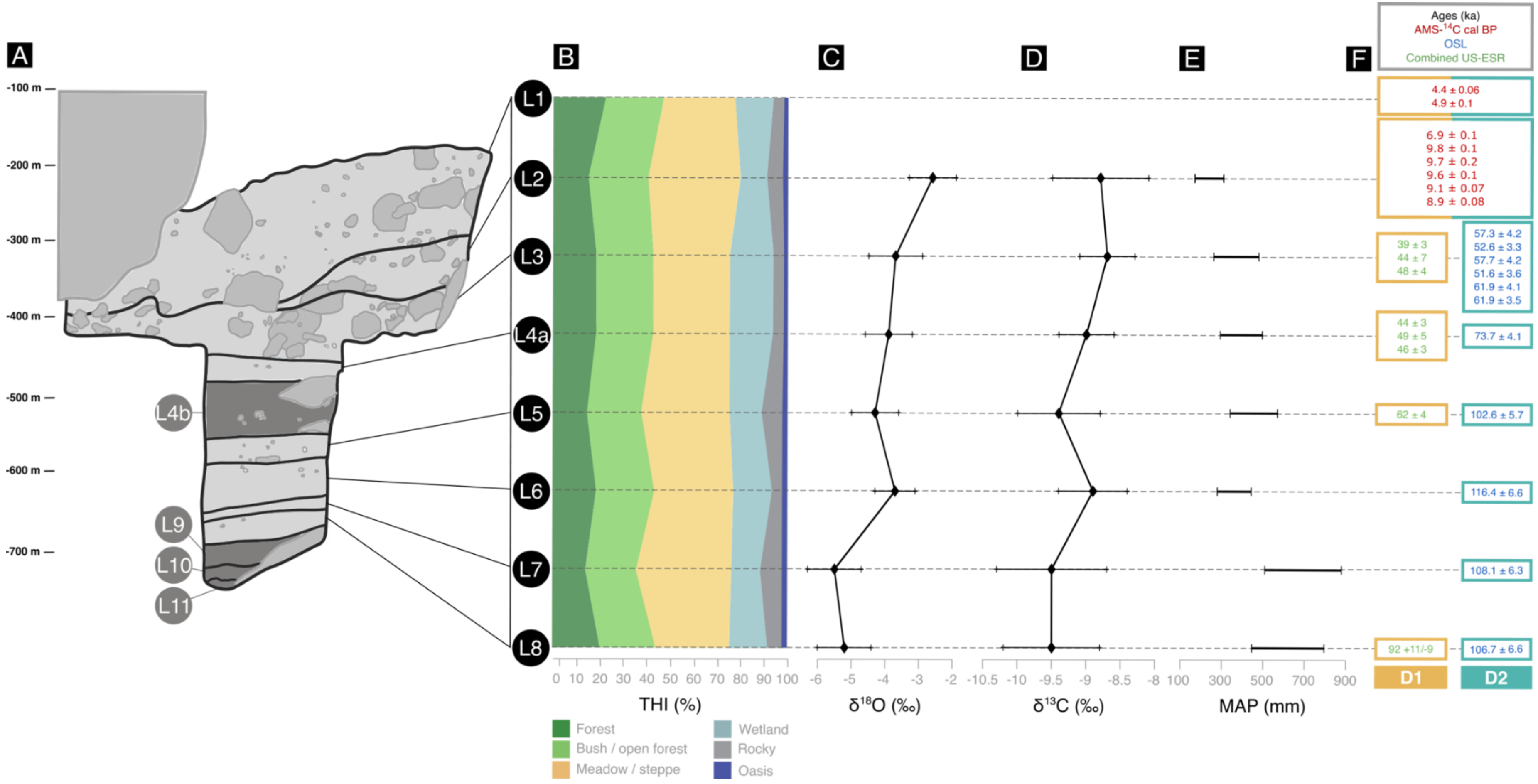

Fig. 2. Summary diagram displaying stratigraphy, paleoenvironmental proxies and the two dating hypotheses of El Harhoura 2 (EH). **A**: stratigraphy of EH, unused layers are in dark grey; **B**: relative % of THI values (adapted from Stoetzel *et al.* (2014) and Jeffrey (2016)); **C**: mean δ^{18}O values in *Meriones* teeth (from Jeffrey (2016)); **D**: mean δ^{13}C values in *Meriones* teeth (from Jeffrey (2016)); **E**: Mean Annual Precipitation (MAP; from Jeffrey (2016)); **F**: dating hypotheses D1 (brown) and D2 (blue) for the different layers of EH (Nespoulet & El Hajraoui, 2012; Jacobs *et al.*., 2012; Janati-Idrissi *et al.*, 2012; Ben Arous *et al.*, 2020b, a; Marquer et al., 2022).

2.1.2 Chronostratigraphy and dating hypotheses

EH displays a high resolution stratigraphy and its layers have revealed an impressive taxonomic richness and delivered an important amount of large and small vertebrate remains (Michel et al., 2009; Stoetzel et al., 2011, 2012b). Its stratigraphy is currently divided into 11 layers (**Fig2 A**) (each layer is abbreviated as "L" followed by the layer number, and for consistency current days is referred as "L0"), among which eight are well studied and considered in this study. All of these eight layers have been dated (Ben Arous et al., 2020b). Three different methods were used: AMS-^{14}C (Nespoulet and El Hajraoui, 2012; Marquer et al., 2022), OSL (Jacobs et al., 2012) and combined US-ESR (Janati-Idrissi et al., 2012; Ben Arous et al., 2020a). AMS-^{14}C is the most reliable dating method of the three and is used for recent layers (L1 and L2). However, for older layers beyond the reach of AMS-^{14}C (L3, L4a, L5, L6, L7 and L8), OSL and combined US-ESR method are used. However, when applied to a same layer, these two methods present discrepancies. For example, it is the case of L5 dated at ~60 ka by combined US-ESR and at ~100 ka by OSL (**Fig2 F**). In addition, when two consecutive layers are dated with these different methods, dates can be inconsistent with the relative position of the layers in the stratigraphy, as it is the case for the L8 dated at ~90 ka using combined US-ESR and L7 at ~110 ka using OSL (**Fig2 F**). To overcome this issue, we choose to set two separate dating hypothesis or the stratigraphic sequence: D1 refers to the chronological sequence based on AMS-^{14}C and combined US-ESR dates, and D2 on AMS-^{14}C and OSL dates. The DH are presented on **Fig2 F**.

2.1.3 Paleoenvironmental variables

Paleoenvironments at EH have been inferred based on two different kinds of proxies: species presence and stable light isotope composition. Regarding species presence, paleoenvironments are reconstructed using the Taxonomic habitat index (THI). The THI is a palaeoecological index which allows one to reconstruct the paleolandscape based on the species composition of the community (Stoetzel, 2009; Stoetzel et al., 2011, 2014). Each species is associated to its preferred habitat based on the assumption that species' ecological preferences were the same in the past as they are today. From that is deduced a qualitative composition of the paleolandscape, expressed as a percentage. Data are from Stoetzel et al.

(2014) and are presented in **Fig2 B**. Note that the oasis habitat was not considered because its percentage of presence does not vary over the EH sequence.

Isotope-based inferences are from *Meriones* teeth. They provide information about the diet and the environment of studied individuals (Longinelli and Selmo, 2003; Navarro et al., 2004; Royer et al., 2013). Two isotopic fractions are considered: $\delta^{18}O$ and $\delta^{13}C$. Plants consumed by small mammals are sensitive to environmental conditions which shows up in their $\delta^{13}C$ and $\delta^{18}O$ values. Because of that, they are good indirect indicators of aridity, seasonal variation and vegetal cover (Longinelli and Selmo, 2003; Blumenthal et al., 2017; Blumenthal, 2019). We used $\delta^{18}O$ and $\delta^{13}C$ means, minimums and maximums, and reconstructed mean annual precipitation (MAP) computed from $\delta^{18}O$ from Jeffrey (2016). Data are presented in **Fig2 C, D** and **E**.

2.2 Paleoclimate simulations

2.2.1 Climate model and experiments

We ran a new set of paleoclimate simulations covering the Late Pleistocene to mid-Holocene period using the model LMDZOR6A (Hourdin et al., 2020). This model is the atmosphere-land surface component of the IPSL-CM6A-LR coupled model (Boucher et al., 2020) that has been used to run the CMIP6 ensemble of past, present and future coupled climate simulations (Eyring et al., 2016), including the mid-Holocene (Braconnot et al., 2021), last interglacial (Sicard et al., 2022; Otto-Bliesner et al., 2021) and Pliocene (Haywood et al., 2016) periods. It has an atmospheric resolution of 144 points in longitude, 143 points in latitude and 79 vertical levels (144x143xL79). Compared to previous IPSL model version it has a finer spatial and vertical resolution and an improved representation of atmospheric and land surface processes. In addition, the simulated climatology of temperature and precipitation over the region is consistent with observations when the model is run for present day conditions with sea-surface temperature prescribed to the monthly climatology of the observed Atmospheric Model Intercomparison Project (AMIP) SST fields (Boucher et al., 2020, 2018) **(Fig 1** and **3)**. Comparison of the simulated annual mean cycle of surface air temperature and precipitation match quite well the observed one, despite an overestimation of summer temperature and sligh 0-1 month shift in the seasonal cycle of precipitation (**Fig3**).

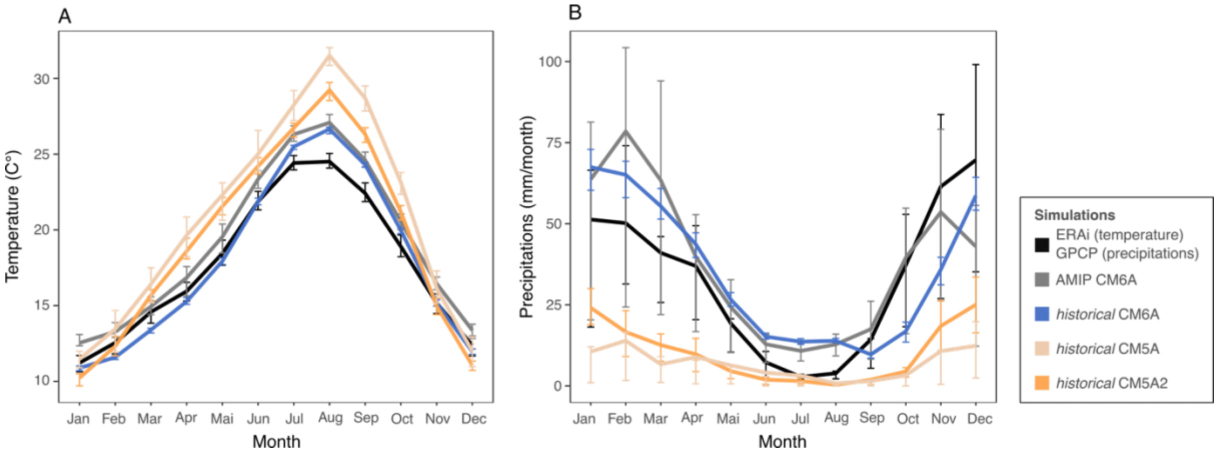

Fig. 3. Monthly variations in mean temperature (unit: C°) and precipitation (unit: mm/month) of the ERAi and GPCP reanalyzed data, the AMIP CM6A simulations (atmosphere only) and *historical* coupled simulations of IPSL-CM5A-LR, IPSL-CM5A2-LR and IPSL-CM6-LR models on the four grid cells containing EH cave. Data were averaged on 30 seasonal cycles (1980-2009). Error bars are estimated from interannual variation over the averaged 30 years and is visualized by quartiles. As a reference for current climate we used monthly data from the global atmospheric reanalysis ERA-interim for monthly mean temperature (Berrisford et al., 2011) and from the GPCP v2.3 (Global Precipitation Climatology Project) for monthly mean precipitation (Adler et al., 2018).

We produced a total of six paleoclimate simulations with the LMDZOR6A model for the key periods of the EH sequence: *midH* (for the mid-Holocene period), *earlyH* (for the early Holocene period), *midMIS3* (for the mid MIS3 period), *lateMIS4* (for the late MIS4 period), *midMIS4* (for the mid MIS4 period) and *MIS5d* (for the MIS5d period). The different simulations differ by prescribed Earth's orbital parameters, atmospheric trace gases composition, ice-sheet configuration and sea surface temperature (SST) in order to represent the climate conditions of the different periods (see **Table 2** for details). For this we make use of preexisting paleoclimate and control simulations that have been run in the last 8 years with different versions of the IPSL model (Marti et al., 2010; Dufresne et al., 2013; Boucher et al., 2020) (details are available in **Table 1**). For all these simulations the vernal equinox is prescribed to occur on March 21 at noon following the paleoclimate modeling intercomparison project (PMIP, Kageyama et al., 2018) recommendations.

Table. 1. Preexisting coupled simulations from the IPSL repository.

Model	IPSL-CM6A-LR	IPSL-CM5A-LR	IPSL-CM5A-LR	IPSL-CM5A-LR	IPSL-CM5A-LR	IPSL-CM5A2-LR
Date	~ 6 kyr BP	~ 9 kyr BP	~ 40 kyr BP	~ 60 kyr BP	~ 66 kyr BP	~ 115 kyr BP
References	Kageyama et al. (2017) Braconnot et al. (2021)	Le Mézo et al. (2017)	Le Mézo et al. (2017)	Le Mézo et al. (2017)	Le Mézo et al. (2017)	Sicard personal communication

We also ran a control simulation *Ctrl* (see **Table 2** for details), representative of the present-day climate. The Sea Surface Temperature (SST) boundary conditions used in *Ctrl* correspond to the mean annual cycle of the SST estimated from current observations used for the AMIP (Boucher et al., 2018) and repeated in time. This *Ctrl* simulation will be considered as the reference for the current climate in our ensemble of new atmospheric simulations.

Unfortunately, simulated paleoclimate SST are not directly comparable because they were performed using different versions of the IPSL model (**Table 1**). This is due to the fact that the various versions of the model are characterized by different physical representations, resolutions and tuning. In particular, these different model versions show different present-day SST biases when compared to observations (**Fig 4**). They translate in different representation of the seasonal cycle of surface air temperature and precipitation at EH in simulations with LMDZOR6 when used as boundary condition instead of the AMIP SST field (**Fig 3**). The magnitude of the seasonal cycle is overestimated and precipitation are underestimated with almost no seasonality when IPSLCM5A or IPSLCM5A2 control SST are used as boundary condition. This differences that can be attributed exclusively to the differences in the SST biases are significant and may deteriorate the simulation of other variables of interest, thus complicating the intercomparison between our new LMDZOR6A simulations. Indeed, the differences between these simulations for the periods of interest at EH could then result from the difference in bias between the various versions of the model rather than representing significant climate differences between periods. In order to produce an homogeneous set of simulations we thus apply a correction to the SST fields (described below) to that the results better fit the observations for present day and the information of the SST changes for the different period is kept as part of the prescribed paleoclimate SST boundary conditions.

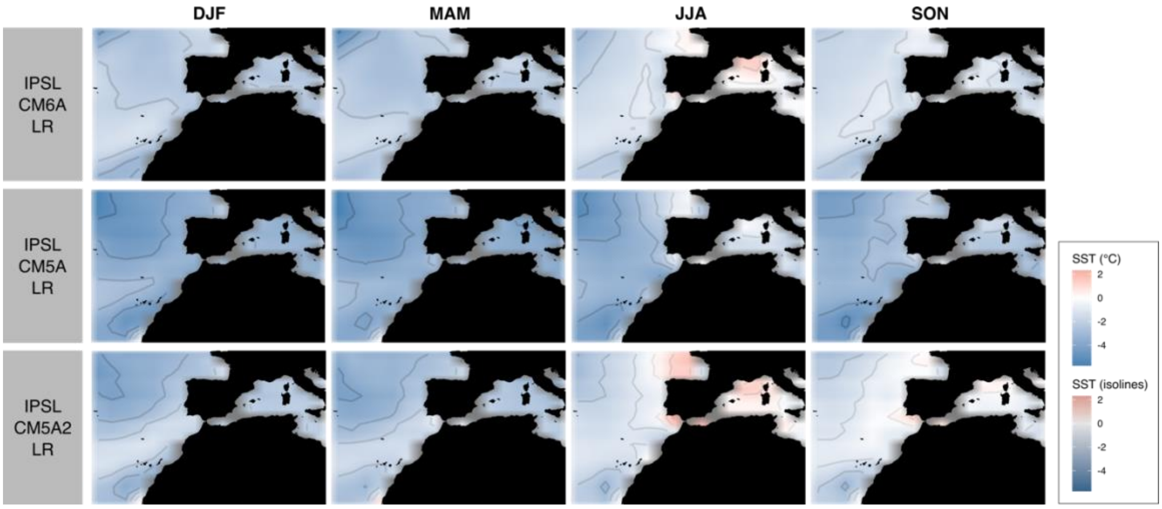

Fig. 4. SST biases of IPSL-CM5A-LR, IPSL-CM5A2-LR and IPSL-CM6A-LR relative to AMIP's SST (issued from current observations) (unit: °C). The seasons are DJF: December, January, February (winter); MAM: March, April, May (spring); JJA: June, July, August (summer); SON: September, October, November (autumn).

2.2.2 Sea-surface boundary conditions

We correct the simulated SST of each coupled simulation for the systematic bias of the model. This is done by removing the SST bias corresponding to the model version used. In other words, corrected SSTs were obtained according to the formula:

$$\text{SSTcor} = \text{SSTsim} + (\text{SSTamip} - \text{SSTmod})$$

Where SSTsim are the SSTs from the coupled simulation, SSTamip are the AMIP SSTs, SSTmod the SSTs of the model version for current days and SSTcor the corrected SSTs, which will be used as boundary conditions in our new LMDZOR6A simulations. The underlying assumption in this correction scheme is that the mean annual SST bias cycle, e.g. SSTmod – SSTamip for each, is stationary in time.

Note also that boundary conditions files of pre-existing (coupled) simulations were interpolated on a 143x144xL79 grid to be compatible with the grid of LMDZOR6A. The corrections are applied to daily SST values of the modern climate, so that the changes in season from the orbital parameters are properly accounted for in the new daily SSTs imposed as boundary condition given the way the vernal equinox is prescribed in the model.

Configuration details for the new set of simulations are summarized in **Table 2**. The length of all these new simulations is 50 years, which is long enough given the fact that LMDZOR6A is an atmospheric model. In the following annual mean cycles are estimated from the last 30 years of each LMDZOR6A simulation.

Table. 2. Forcing and boundary conditions of the simulations produced in this study.

Simulations							
Name	***Ctrl***	***midH***	***earlyH***	***midMIS3***	***lateMIS4***	***midMIS4***	***MIS5d***
Model	LMDZOR6A	LMDZOR6A	LMDZOR6A	LMDZOR6A	LMDZOR6A	LMDZOR6A	LMDZOR6A
Date	Current days	~ 6 kyr BP	~ 9 kyr BP	~ 40 kyr BP	~ 60 kyr BP	~ 66 kyr BP	~ 115 kyr BP
Orbital parameters*							
Eccentricity	Same as *clim_pdControl*	0.018682	0.01935	0.016715	0.018469	0.021311	0.041421
Obliquity (degrees)	Same as *clim_pdControl*	24.105	24.231	23.441	23.2329	22.493	22.404
Perihelion – 180	Same as *clim_pdControl*	0.87	303.03	102.7	266.65	174.82	110.88
Solar constant (W/m2)	Same as *clim_pdControl*	Same as *clim_pdControl*	Same as *clim_pdControl*	1365.6537	1365.6537	1365.6537	1361.20
Gaz concentration							
Carbon dioxide (ppm)	Same as *clim_pdControl*	264	287	205	230	195	274
Methane (ppb)	Same as *clim_pdControl*	597	791	500	450	450	505
Nitrous oxide (ppb)	Same as *clim_pdControl*	262	275	260	230	217	251
SST	Same as *clim_pdControl*	Simulated tsol_oce from pre-existing simulations (corrected for the models' systematic bias)					
Geography	Same as *clim_pdControl*	Same as pre-existing simulations					
Vegetation	Same as *clim_pdControl*	Same as pre-existing simulations					

* The term "orbital parameters" refers to variations in the eccentricity of the Earth and longitude of perihelion as well as changes in its axial inclination (obliquity).

2.2.3 A subset of key paleoclimate variables

To characterize the large-scale climate over the area, we worked on the mean annual cycle of the four grid cells containing EH. From simulations *Ctrl*, *midH*, *earlyH*, *midMIS3*, *lateMIS4*, *midMIS4* and *MIS5d* we extracted nine output variables. We choose to focus on variables that are likely to directly or indirectly influence the landscape and/or biotic environment. Based on a review of the ecological literature, we selected: *tsol* (temperature at surface, in C°) (Gillooly et al., 2001; Yom-Tov and Geffen, 2006; Ebrahimi-Khusfi et al., 2020), *precip* (precipitation, in mm.month^{-1}) (Yom-Tov and Geffen, 2006; Alhajeri and Steppan, 2016; Ebrahimi-Khusfi et al., 2020), *qsurf* (specific humidity, in kg.kg^{-1}) (Hovenden et al., 2012; Alhajeri and Steppan, 2016), *w10m* (wind speed at 10 meters, in in m.s^{-1}) (McNeil, 1991; Tanner et al., 1991; Chapman et al., 2011; Pellegrino et al., 2013), *sols* (solar radiation at surface, in W.m^{-2}) (Monteith, 1972; Fyllas et al., 2017), *drysoil_frac* (fraction of visibly dry soil, in %) (Paz et al., 2015) and *humtot* (total soil moisture, in kg.m^{-2}) (Paz et al., 2015). Two additional variables were computed. The diurnal temperature range *tsol_ampl_day* (in C°; Alhajeri and Steppan, 2016) computed from *tsol_max* (day maximum temperature) and *tsol_min* (day minimum temperature) as: *tsol_max – tsol_min*; and the hydric stress *hyd_stress* (in mm.day^{-1}; Martínez-Blancas and Martorell, 2020) computed from *evapot* (potential evaporation) and *evap* (evaporation) as: *evapot – evap*.

We explore variations in annual means (mean value of the variable) and annual standard deviations (amplitude of seasonal variation). The means and standard deviations are computed on the annual mean cycle estimated from the last 30 years of each LMDZOR6A simulations, thus they represent respectively the annual mean and the seasonal amplitude of the variable. In all analyses, climate variables were standardized between periods.

Potential biases related to calendar effect (the change of length of seasons and month between periods (Bartlein and Shafer, 2019; Joussaume and Braconnot, 1997)) were considered and discounted in the statistical analyses by caracterising the annual mean cycles by their annual means and standard deviations. Indeed, these metrics are slightly, if at all, affected by the calendar effet, in particular when they are properly weighted by the number of days in the months (estimated using the modern or a celestial calendar). This choice is made to keep the physical consistency between the different variables that nonlinearly depend on moisture and temperature.

The association of paleoclimate simulations with the stratigraphic layers of EH is based on age proximity. This step is performed for both D1 and D2 (the DH presented in section 2.1.2). As a result, we obtain two hypothetic paleoclimate sequences corresponding to EH sequence.

In order to easily visualize the climate proximity/differences between EH layers we used a principal component analysis (Jolliffe and Cadima, 2016). This analysis allows one to find new uncorrelated variables that successively maximize variance (the principal components). They are computed from the eigenvectors and eigenvalues of the covariance/correlation matrix (correlation matrix in our case, as all the variables are standardized). Then, the data can be visualized along the leading principal components, which maximizes the amount of information displayed. It allows us to visualize EH layers along the two main axis of variance in climate data, resulting in that the proximity of stratigraphic layers in the plot represents the proximity between the climate of the layers. The principal component analyses are performed on the annual mean and standard deviations (seasonal amplitude) of climate variables.

2.3 Consistency analyses

To test the consistency between the paleoclimate simulations and paleoenvironmental inferences that have been made from the content of the EH site we use two kind of analyses: two-block Partial Least Squares (2B-pls) and pairwise correlation tests. For these analyses, the climate variables are the principal components provided by the principal component analysis described above. Working on principal components instead of original variables allow us to remain in a multivariate framework and thus to take into account the interrelationships between climate variables. This while considering separately the uncorrelated axes of variance (principal components), which may display different covariation with the paleoenvironmental indicators. The different paleoenvironmental proxies considered are $\delta^{18}O$ and $\delta^{13}C$ means, minimums and maximums, and MAP, as well as percentages of represented habitats indicated by the THI.

The 2B-pls tests the global covariance between climate variables and paleoenvironmental variables. This multivariate method explores patterns of covariation between two sets of variables, i.e. two blocks

(Sampson et al., 1989; Streissguth et al., 1993). Axes of maximum covariance between the two blocks are generated, thus reducing data dimensionality. A coefficient (r-PLS) is computed and represents the strength of covariation. The r-PLS is in the range of (0,1). The closer the r-PLS is to one, the stronger the covariation. P-values indicating the statistical significance of r-PLS were calculated based on 1000 permutations against the null hypothesis (absence of covariation between the two sets of variables). Then, to refine our results, we performed pairwise correlation tests.

3 Results

3.1. Simulated climate changes

Changes in atmospheric circulation and pressure over the sequence are presented in **Fig 5**, and plots of monthly precipitation and temperatures for the region of EH are available in **Fig 6**. The proximity between the climate of each period and the current climate is showed on similarity maps on **Fig 7**. We didn’t account for the calendar effect in these graphs, however they are only there to illustrate the major differences between the periods, that are not affected by it.

The atmospheric circulation over the region differ between winter and summer. Winter is marked by a meriodional pressure gradient and dominated by a zonal flow from west to east. In summer, the pressure gradient is more horizontally-oriented, with the establishment of a depression on the North African continent and the northward drift of high pressures on the Atlantic Ocean (**Fig 5**). All over the sequence, these processes shift slightly, especially between *lateMIS4, midMIS4, midMIS3* (period from ~66ka to ~40ka) and *Ctrl, midH, earlyH* (period from ~9ka until today) (**Fig 5** and **7**), at the exception of *MIS5d* (~115ka) which conditions are relatively close from current ones on **Fig 7**. There are also important changes in the magnitude of the seasonal temperature variation from June to October and of the seasonal precipitation variation from October to May between these two major periods (**Fig 6**).

From ~115ka (*MIS5d*) until ~40ka (*midMIS3*), the climate was colder than today. From ~66ka (*midMIS4*) to ~40ka (*midMIS3*), there is also more precipitation in winter (**Fig 6**). These conditions share similarities with what can be found in slightly higher latitudes today (**Fig 7**), it is consistent with the pressure along the North Africa (and Morrocan) coast (**Fig 5**). In ~115ka (*MIS5d*), conditions are also cold, but as dry as in the Holocene (**Fig 5**). They are not related to changes in the atmosphere circulation (**Fig 5**) but rather to changes in insolation, with current analogs limited to North Africa (**Fig 7**). Starting from ~9ka (*earlyH*) the seasonal temperature variation is enhanced. Conditions in winter and spring are similar to the current climate (**Fig 7**), but with a warmer autumn and a much warmer summer (**Fig 6**). At ~6ka (*midH*), climate conditions are close from today (**Fig 7**), but with a slightly more important seasonal temperature variation (**Fig 6**).

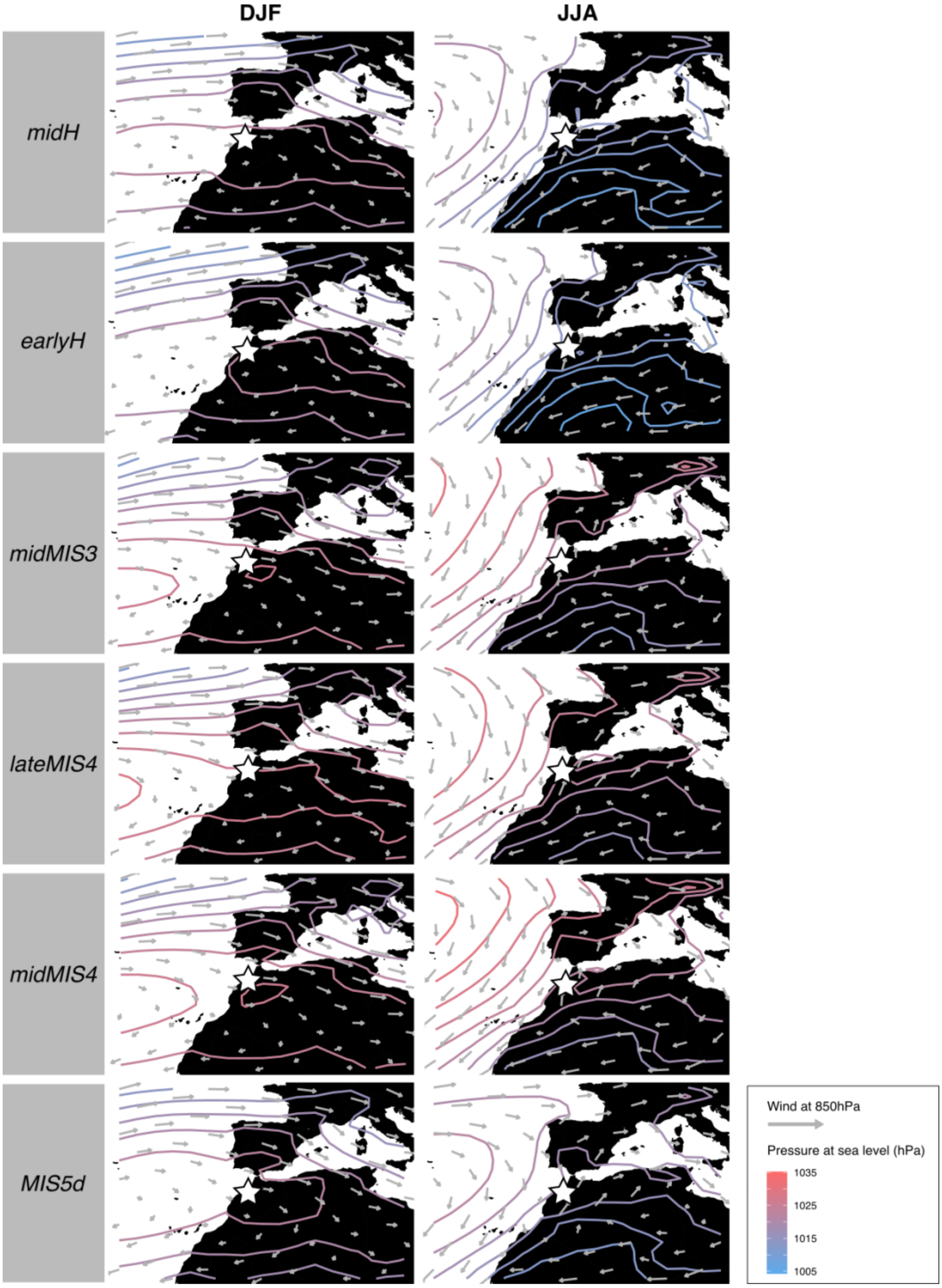

Fig. 5. Maps of wind speed and direction at 850hPa (represented by arrows, length is proportional to wind speed) and corrected pressure at sea level (unit: hPa) per season simulated with *midH*, *earlyH*, *midMIS3*, *lateMIS4*, *midMIS4* and *MIS5d*. EH cave location is represented by a star in the upper left panel. DJF: December, January, February (winter); JJA: June, July, August (summer).

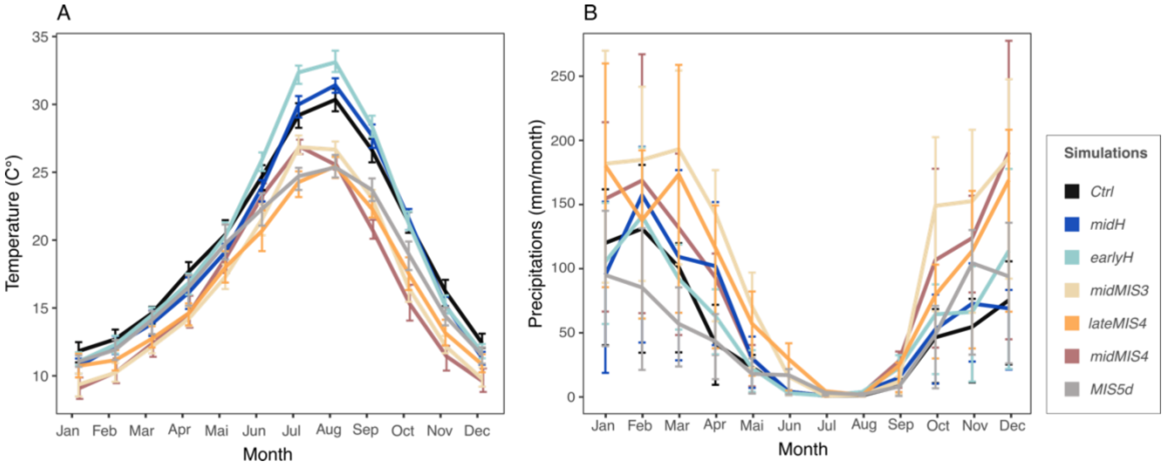

Fig. 6. Graph of monthly variations in mean temperature (unit: °C) and precipitation (unit: mm/month) averaged from the four grid cells containing EH cave in the different simulations. Interannual variation over the averaged 30 years is visualized by quartiles.

3.2 Consistency between paleoclimate simulations and paleoenvironmental inferences

3.2.1 Association of paleoclimate simulations and stratigraphic layers

The two hypothetic paleoclimate sequences corresponding respectively to D1 and D2 are presented in **Fig 8**. The two principal components analyses are shown in **Fig 9**. To visualize how climate variables are associated to structure the climate-space of these two principal component analyses, biplots are available in **SM Fig 2.**

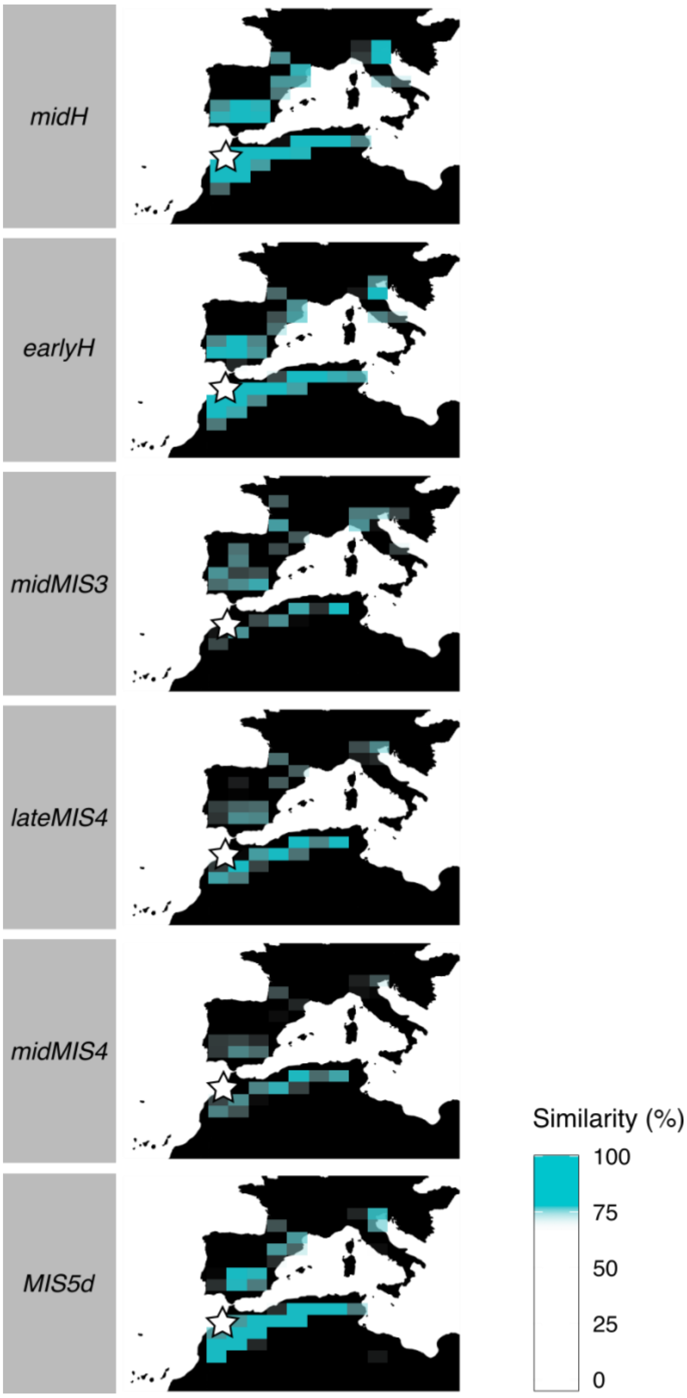

345 **Fig. 7.** Maps presenting the similarity between past climates on EH and current climate on the area. For each cell in the *Ctrl* simulation, we computed the Euclidean distance between the climate variables (means and standard deviations) associated to the cell and the climate variables on the four cells containing EH of each past period. Blue cells indicate localities where current climate is more than 75% similar to past climate on EH (blue scale indicates the degree of similarity). EH cave location is 350 represented by a star in the upper left panel.

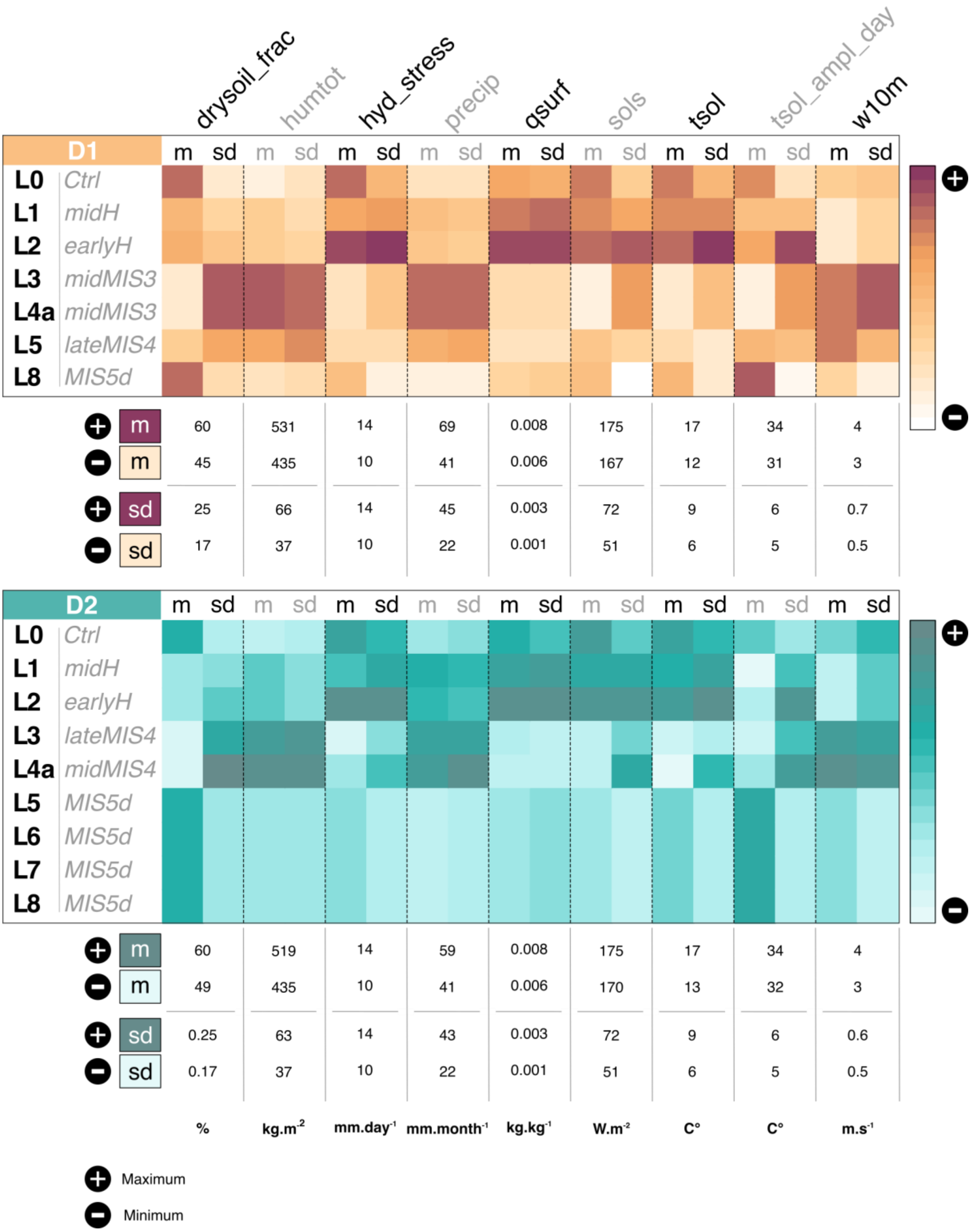

Fig. 8. Climate variation over the EH sequence according to D1 (Dating Hypothesis 1; in brown), and D2 (Dating Hypothesis 2; in blue). The color scales reflect the intensity of the variables: an intense color (brown for D1, blue for D2) indicates a maximum, while a clear (white) color a minimum.

Maximum/minimum (+/-) refers to the range of values explored by each variables with their original unit across simulations. “L” is the abbreviation for Layer, “m” for mean and “sd” for standard deviation.

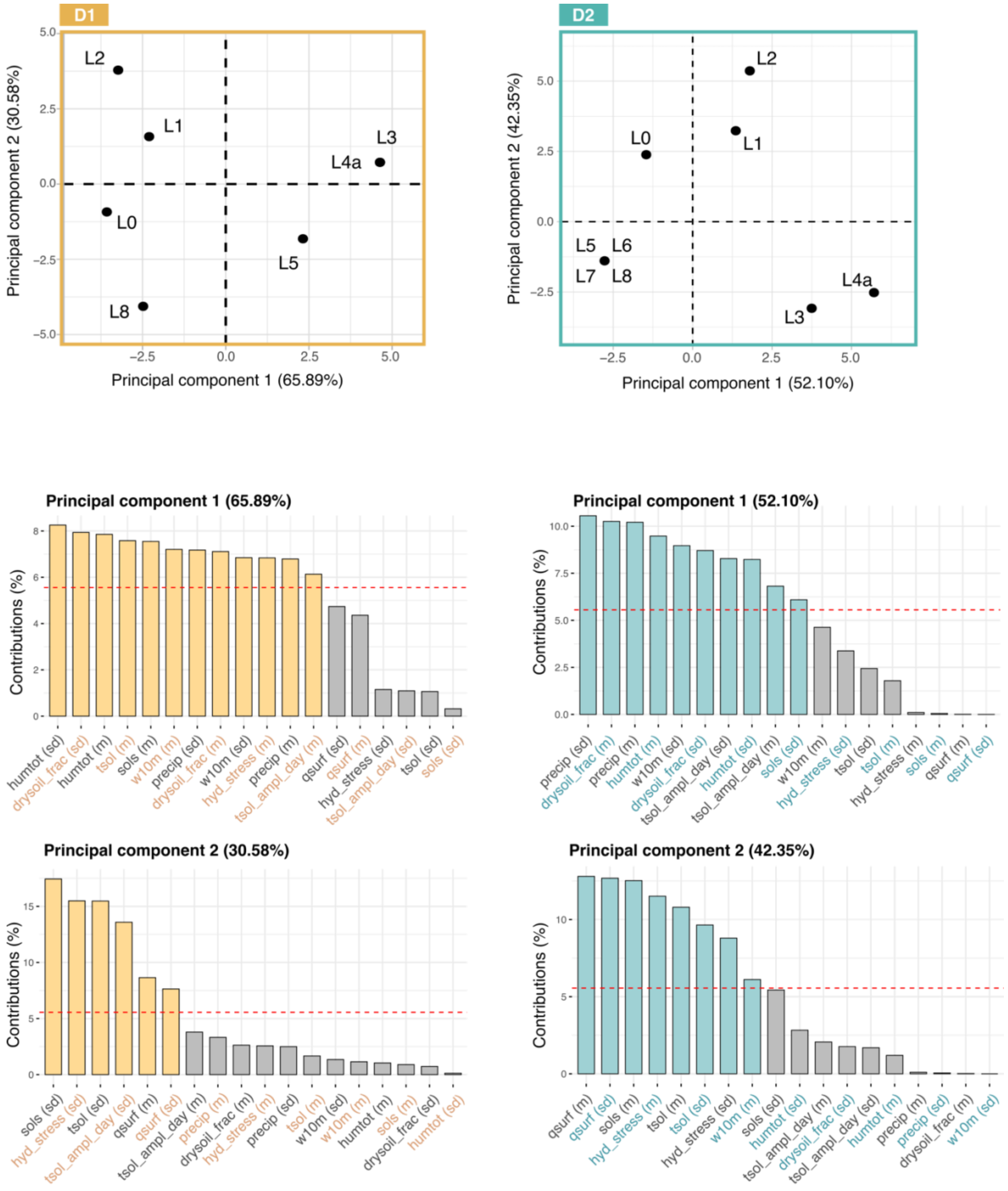

Fig. 9. Principal component analyses performed on climate variables according to D1 (Dating Hypothesis 1; in brown), and D2 (Dating Hypothesis 2; in blue). The axes represent the two leading

principal components (along which data are visualized), and the numbers in parentheses are the percentage of variance carried by each axis. The barplots below each graphare the contributions of the (standardized) climate variables to the two leading principal components (variables above the horizontal red line contribute significantly). “L” is the abbreviation for Layer. To better distinguish the variable names, they are presented with two colors (black and the color corresponding to the dating hypothesis).

Based on D1, our results indicate four major climate transitions (**Fig 8**). The first occurs between L8 and L5. In L5 the climate is wetter and colder with more precipitation, more soil humidity, increased wind speed, less hydric stress and less portions of dry soil. Humidity, precipitation and wind speed also show an important seasonal variability. The second transition, less marked, is between L5 and L4a. Climate in L4a is rather similar to the climate in L5, but precipitation and humidity have increased. Seasonal variations are globally more pronounced. The third transition is between L3 and L2. The climate changes drastically between these two periods, with hotter and drier conditions in L2 corresponding to the end of the last deglaciation. Temperature, solar radiation, water stress and soil dryness all increase, coupled with a decrease in precipitation, soil moisture and wind speed. All these changes are consistent with aridification or desertification from L2. Surprisingly, however, specific humidity is enhanced, which is partly consistent with the decrease in precipitation and wind speed at this coastal location, and is concomitant with large changes of the atmospheric circulation patterns over this region from L2 (**Fig 5**). The last climatic transition is more subtle and occurs between L1 and Act. The environment in Act seems closer to the one in L8 with more seasonal variability in temperature, solar radiation and water stress (**Fig 8**).

Overall, there is an alternation of two main climate types. This partition is confirmed by the principal component analysis shown in **Fig 9**. The first principal component explains 65.85% of the observed variance (of the standardized variables) and splits the layers of EH into two climate regimes. The first regroups L3, L4a and L5 and is defined by humid and windy conditions with a high seasonal variability. The second includes Act, L1, L2 and L8 and is characterized by hot and dry conditions. The second axis, explaining 30.28% of the variability, divides the latter group into two subgroups: L1 and L2 with high seasonal variability, and Act and L8 with a lower seasonal variability.

Regarding D2, we observe three important and abrupt climatic transitions (**Fig 8**). The first happened between L5 and L4a. In L4a, the climate is much windier and temperatures are colder with a substantial increase of diurnal temperature range. Precipitation and soil moisture increase importantly while hydric stress decreases. The climate also presents an overall higher seasonal variability. These tendencies persist in L3. The second transition is between L3 and L2. The soil is drier and the hydric stress increases greatly as well as solar radiation and temperature. Precipitation and soil moisture are less important. Conditions in L1 are close from those in L2, a bit colder with a less marked water stress. The last climate transition, smoother than the previous ones, occurs between L1 and Act and is mainly marked by a global decrease of seasonal variations.

Results associated with D2 suggest that three types of climate succeeded one another at EH. The first group is composed of L8, L7, L6 and L5, the second by L3 and L4a and the third by L2, L1 and Act. As for D1, this partition is supported by the principal component analysis results presented in **Fig 9**. The first principal component, which explains 52.10% of the observed variance, separates the group containing L8, L7, L6 and L5 with the one composed of L3 and L4a. The second principal component, explaining 42.35% of the observed variance, separates the group of L2, L1 and Act from others. L8, L7, L6 and L5 are characterized by a hot and dry climate and a low seasonal variation. L3 and L4a are defined by a wet and windy climate, with important precipitation and high seasonal variability. Finally, L2, L1 and Act present a hot environment associated with an important water stress.

3.2.2 Consistency analyses

Results of 2B-pls and pairwise correlations between climate and paleoenvironmental variables are presented in **Fig 10**. Regarding D1, no significant covariation is found between THI values and climate variables. However, 2B-pls shows that there is a statistically significant covariation between isotope data and all climate variables, and between isotope data and the second principal component (climate variables contributing to the second principal component are indicated in **Fig 9**). Specifically, this second principal component is positively correlated with $\delta^{18}O$ mean, maximum and minimum values and $\delta^{13}C$ maximum values. Conversely, D2 presents no statistically significant result for 2B-pls nor correlations, meaning that for D2 paleoclimate inferences and paleoenvironmental proxies are not consistent.

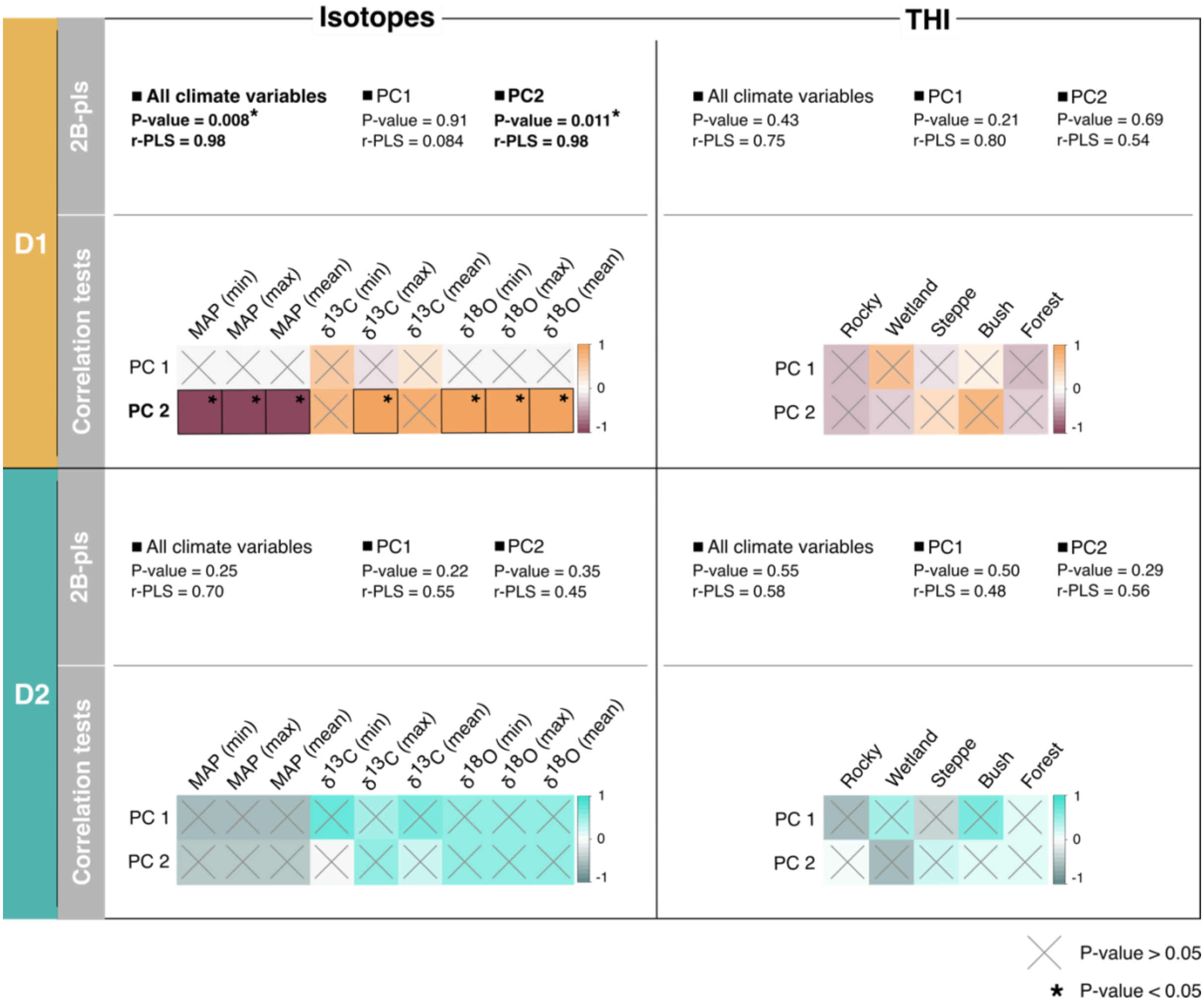

Fig. 10. Results of the 2B-pls and correlations tests performed between isotopes (Jeffrey, 2016) and THI values (Stoetzel *et al.*, 2014), and climate variables according to D1 (Dating Hypothesis 1; in brown), and D2 (Dating Hypothesis 2; in blue). Statistically significant results (p-value < 0.05) are indicated by (*). Regarding correlations tests, crosses indicate cases where correlation is not significant (p-value > 0.05) and colors represent the strength of the correlations. For isotopes: $\delta^{18}O$ and $\delta^{13}C$ values are from *Meriones* teeth (from Jeffrey (2016)) and MAP is the Mean Annual Precipitation (from Jeffrey (2016)).

For THI: Forest, Bush, Steppe, Wetland and Rocky refer to relative % of the representation of environmental types according to the THI (from Stoetzel *et al.* (2014) and Jeffrey (2016)).

4 Discussion

Despite the differences in scale and resolution between climate and paleoenvironmental data, we find statistically significant and meaningful results. The climate changes considered seem to be large enough for a consistency to be detected between the climate and environmental data. First, we discuss the paleoclimate changes described by simulations over the period, and the underlying dynamical processes. Then, we address the contribution of climate simulations to the discussion of chronological and paleoenvironmental discrepancies of EH.

4.1 Paleoclimate variation and underlying forcings

Paleoclimate simulations allow us to discuss several important climate changes at EH over the Late Pleistocene to mid-Holocene period. These paleoclimate variations may result from the mixed influence of global and regional dynamical processes.

The variation of radiative-related variables (as sols, tsol or tsol_ampl_day) seems to depend more on global processes related to large-scale climate changes. They clearly separate interglacial climate (*Ctrl, midH, earlyH*) from glacial climate (*midMIS3, lateMIS4, midMIS4, MIS5d*). The warm/cold differences between these two periods is due to the size of the ice-sheet and variation in gaz concentration. For example, mean insolation and temperature significantly increase in early Holocene relatively to other periods, along with increasing greenhouse gas concentrations and the retreating ice sheet. Also, obliquity and precession of the Earth orbit increases at this period relatively to others, along with the amplitude of the seasonal variability of insolation and temperature. Note that *MIS5d* is a peak of glacial sub-stage where conditions where quite mild, which explains the proximity of its climate with current ones.

The variation of the humidity-related variables (as precip, hydric_stress or drysoil-frac) seems to be mainly explained by a translation of the regional atmospheric circulation processes over the sequence.

For example, mean precipitation and soil moisture are higher from mid-MIS4 to mid-MIS3. At this time, the wet and cold westerly winds descend further south and blow across the area of EH. This is explained by the position of the Açores High: the magnitude of the high pressures creates a stronger pressure gradient, thus favoring a stronger zonal circulation, which brings cooler and more humid air on the North African coast. Therefore, for this region, the atmospheric circulation effect and changes in moisture advection over the region have a significant impact on whether a warmer climate would lead to increased moisture content and precipitation.

4.2 Paleoclimate simulations and chronostratigraphy

The climate sequence differs significantly depending on the DH it is based on. Based on D1, there is an alternation of semi-arid and temperate climates. The climate succession based on D2 is quite different, with the presence of three main climate types and rapid transitions between them. The climate sequences based on D1 and D2 are not equally congruent with paleoenvironmental proxies from the literature. Indeed, several statistically significant correlations and covariation are found between the climate sequence based on D1 and the paleoenvironmental inferences, while none are found for the one based on D2. Thus, our results suggest that, with respect to EH, combined US-ESR dating may be more reliable than OSL dating. As this dating process relies on quartz grains and that their chronology and origin is difficult to establish in the context of karstic coastal caves (as discussed in Ben Arous *et al.* (2020a)), OSL ages might have been overestimated (i.e. the age of the layers may be younger than estimed by OSL). Moreover, OSL dates can in some cases be internally inconsistent, meaning that they can have a number of reversals. For instance, it is known that water content influences the determinations. Considering the location of the cave on the coastline, inundations related to rising in sea level or very high tides may have occurred.

4.3 Paleoclimate simulations and paleoenvironmental inferences

Because the climate sequence based on D1 is the only one displaying significant results, we focus on it in the following discussion. Isotope fractions are mainly correlated to seasonal variation in water stress (hyd_stress), insolation (sols) and temperature (tsol, tsol_ampl_day). This result is expected because $\delta^{18}O$ is an indicator of aridity (Longinelli and Selmo, 2003; Blumenthal et al., 2017; Blumenthal, 2019) and $\delta^{13}C$ is related to seasonal variation of temperature and water stress (O'Leary, 1988; Lin, 2013; Smiley et al., 2016). On the contrary to isotopes, the THI is not related to climate variations. It is not completely surprising, as THI is a qualitative estimate of the global type of the environment provided by the whole microvertebrate communities. It is therefore very dependent on the species included in the estimate. Conversely, isotopes reveal quantitative fluctuations in particular variables that are temperature- and precipitation-related provided by a limited number of individuals of a single species. Thus, they do not deliver information at the same resolution, nor do they estimate it using the same approaches.

Another explanation of the improved correlations between climate and isotope fractions may be that biologically-derived proxies (as the THI) are more complex functions of physical drivers than the isotope signal. Isotopes directly reflect to the magnitude of seasonal variation in insolation, water stress, temperature and diurnal temperature range, because these variables condition the presence of essential elements for plants survival (e.g. sunlight, water in the soil). Thus, they are directly related to the type of vegetation. On the other hand, the THI relies on ecological preferences of species. Altogether, the variables of the THI give information about the proportion of biomes (e.g. forest, bush, steppe), and thus the spatial distribution and density of the vegetation. Consequently, its relationship to climate is more indirect than for isotopes.

The large differences between the climate simulations and the fact that they provide a physical consistent view of the relationships between the different climatic variables allow us to discuss the inconsistencies existing between paleoenvironmental proxies at EH. The two major ones concern L5 and L7. In both cases, isotope surveys and MAP from Jeffrey (2016) indicate more humid conditions with more important precipitation than on other layers. On the contrary, the THI as well as the presence of the steppic species *Jaculus* cf. *orientalis* (often used as an indicator of particularly arid conditions) and the scarcity of aquatic species support a drier climate than on other layers (Stoetzel, 2009; Stoetzel et al., 2014). Large mammals would also support this last hypothesis, with an increase in the representation of gazelles and alcelaphines, and a decrease in the representation of bovines in both layers (Stoetzel et al., 2012a, 2014). Unfortunately, no combined US-ESR ages are available for L7 to date. Considering that climate conditions associate to L8 display less precipitation than currently, we could hypothesize a similar climate for L7. In that case, this would support inferences from species presence. Nevertheless, we cannot exclude that a microclimatic event could have induced particular climatic conditions on L7. Concerning L5, the climate described by the sequence based on D1 agrees with isotope surveys (Jeffrey, 2016). These conclusions are supported by the abundance of *Crocidura russula*, a shrew species associated with Mediterranean climates (Cornette et al., 2015). In addition, *Jaculus* cf. *orientalis* can also be considered as an indicator of more continental conditions, such as the distance from the coastline, rather than a marker of arid environments.

An important difference is noticed between the climate sequence and the THI on L1. Paleoclimate simulations indicate on a quite dry climate relatively to other layers, in contradiction with the composition of small and large mammal communities that suggest an expansion of forests and wetlands (Stoetzel *et al.*, 2014). This difference could be explained by the location of EH: the cave is located at the interface of varied climate influences, as described previously. Because global climate models describe general climate characteristics, a local climate phenomenon could have generated a wetter environment in the surroundings of EH.

4.4 Perspectives and limitations of the interdisciplinary approach

The interdisciplinary approach between archeology and paleoclimatology presented in this study opens new avenues for testing the consistency between paleoclimatic simualtions and paleoenvironment reconstructions in different regions. The contextualization of archaeological and paleontological sites could greatly benefit from this approach. Environmental and/or chronological uncertainties such as the ones encountered at EH are unfortunately common in archeology, since the observed differences depend primarily on the methods-specific biases, not especially on the site. However, while the results of this approach are promising in the case of EH, extending it to other sites is only possible under certain conditions. 1) The concerned site must have been well studied and data on the chronology of the sequence must be available from different methods. 2) Paleoenvironmental inferences must also to be available, and preferably from different sources. 3) The stratigraphic sequence must be composed of sufficient levels to allow the application of statistical methods. 4) Fully coupled climate simulations of the periods of interest must be available, otherwise their complete production would represent a considerable amount of work.

While not all sites meet these criteria, a large number of them have been heavily studied and could benefit from our approach, such as other Moroccan sites (Ben Arous et al., 2020b) or sites from the cradle of humankind (Hanon et al., 2019; Pickering et al., 2019). Moreover, with the development of more powerful statistical tools, this approach could even be extended to other sites with less referenced context. Paleoclimate simulations such as the ensemble we used here are becoming more common and distributed, so that their availability should be less a of a concern in the coming years. The most crucial point is to encourage collaboration between the fields of archeology and paleoclimatology, as expertise in both disciplines is needed to properly combine the different types of information.

5 Conclusions

Considering together paleoclimate simulations and paleoenvironmental inferences allows us to provide new insights into the chronostratigraphy and paleoenvironmental reconstruction of El Harhoura 2 cave. We find that the climate sequence based on combined US-ESR ages is more consistent with paleoenvironmental inferences than the climate sequence based on OSL ages. We also show that, overall, isotope-based paleoenvironmental inferences are more congruent with the paleoclimate sequence than species-based inferences. But, above all, we highlight the difference in scale between the information provided by each of these paleoenvironmental proxies. This study demonstrates that the combination of different sources of environmental data and climate simulations has a great potential for refining the paleoenvironmental and chronological context of archeological and paleontological sites. Even so, its applicability on periods marked by less important climate changes remains to be tested. Our approach may concern a limited number of well-studied sites, however with more powerful statistical tools, it could be extended to other sites whose context is less referenced.

Author contribution

Conceptualization: Léa Terray, Pascale Braconnot, Raphaël Cornette, Emmanuelle Stoetzel.

Formal analyses: Léa Terray.

Methodology: Léa Terray, Pascale Braconnot, Masa Kageyama.

Funding acquisition: Léa Terray.

Writing – original draft preparation: Léa Terray.

Writing – review & editing: Pascale Braconnot, Raphaël Cornette, Emmanuelle Stoetzel, Eslem Ben Arous.

Competing interests

The authors declare that they have no conflict of interest.

Code and Data availability

The data and R code that support the findings of this study are openly available on GitHub at https://github.com/LeaTerray/cp-2022-81.git.

Acknowledgments

The microvertebrate remains from El Harhoura 2 cave were recovered and studied within the framework of the El Harhoura-Témara Archaeological Mission (dir. R. Nespoulet and M.A. El Hajraoui), under the administrative supervision of the *Institut National des Sciences de l'Archéologie et du Patrimoine* (Rabat, Morocco) and financial support from the *Ministère des Affaires Etrangères et du Développement*

International (France) and the *Ministère de la Culture* (Maroc). The authors would like to thank Marie Sicard for sharing the *lig115* climate simulation, part of her PhD project. Climate simulations were carried out on the Jean Zay supercomputer at IDRIS and the computing time was provided by the project gen2212. The authors would like to thank Julia Lee-Thorp (School of Archeology, University of Oxford) for sharing her expertise on stable ligtht isotopes and for her suggestions on the manuscript. We are grateful to Pascal Terray (LOCEAN, IRD) for his comments on the manuscript and advice. We also thank the two reviewers, Patrick Bartlein and Chris Brierley, and the editor, Irina Rogozhina, for their kind and helpful comments and suggestions. This research was funded by the Université 463 Paris Descartes, the Ecole Doctorale FIRE – Programme Bettencourt. All operations on NetCDF files (the standard file format for the outputs of the IPSL models) were performed using CDO (Climate Data Operators) (Schulzweida, 2019). Maps, plots and analyses were produced using the R free software (R Development Core Team, 2018) and the libraries *ncdf4* (http://dwpierce.com/software), *raster* (Hijmans and van Etten, 2012), gdata (Warnes et al., 2005), *FactoMineR* (Lê et al., 2008), *factoextra* (Kassambara and Mundt, 2020), *geomorph* (Adams and Otárola-Castillo, 2013), *sp* (Pebesma and Bivand, 2005), *corrplot* (Wei and Simko, 2021), RColorbrewer (Neuwirth, 2014) and *ggplot2* (Wickham, 2015).

References

Adams, D. C. and Otárola-Castillo, E.: geomorph: an R package for the collection and analysis of geometric morphometric shape data, Methods Ecol. Evol., 4, 393–399, https://doi.org/10.1111/2041-210X.12035, 2013.

Adler, R., Sapiano, M., Huffman, G., Wang, J.-J., Gu, G., Bolvin, D., Chiu, L., Schneider, U., Becker, A., Nelkin, E., Xie, P., Ferraro, R., and Shin, D.-B.: The Global Precipitation Climatology Project (GPCP) Monthly Analysis (New Version 2.3) and a Review of 2017 Global Precipitation, Atmosphere, 9, 138, https://doi.org/10.3390/atmos9040138, 2018.

Alhajeri, B. H. and Steppan, S. J.: Association between climate and body size in rodents: A phylogenetic test of Bergmann’s rule, Mamm. Biol., 81, 219–225, https://doi.org/10.1016/j.mambio.2015.12.001, 2016.

Avery, D. M.: Pleistocene micromammals from Wonderwerk Cave, South Africa: practical issues, J. Archaeol. Sci., 34, 613–625, https://doi.org/10.1016/j.jas.2006.07.001, 2007.

Bartlein, P. J. and Shafer, S. L.: Paleo calendar-effect adjustments in time-slice and transient climate-model simulations (PaleoCalAdjust v1.0): impact and strategies for data analysis, Geosci. Model Dev., 12, 3889–3913, https://doi.org/10.5194/gmd-12-3889-2019, 2019.

Ben Arous, E., Falguères, C., Tombret, O., El Hajraoui, M. A., and Nespoulet, R.: Combined US-ESR dating of fossil teeth from El Harhoura 2 cave (Morocco): New data about the end of the MSA in Temara region, Quat. Int., 556, 88–95, https://doi.org/10.1016/j.quaint.2019.02.029, 2020a.

Ben Arous, E., Falguères, C., Nespoulet, R., and El Hajraoui, M. A.: Review of chronological data from the Rabat-Temara caves (Morocco): Implications for understanding human occupation in north-west Africa during the Late Pleistocene., in: Not just a corridor. Human occupation of the Nile Valley and neighbouring regions between 75,000 and 15,000 years ago, edited by: Leplongeon, A., Goder-Goldberger, M., and Pleurdeau, D., Paris, 177–201, 2020b.

Berrisford, P., Dee, D., Poli, P., Brugge, R., Fielding, M., Fuentes, M., Kållberg, P., Kobayashi, S., Uppala, S., and Simmons, A.: The ERA-Interim archive Version 2.0, ERA Report Series, 2011.

Blome, M. W., Cohen, A. S., Tryon, C. A., Brooks, A. S., and Russell, J.: The environmental context for the origins of modern human diversity: A synthesis of regional variability in African climate 150,000–30,000 years ago, J. Hum. Evol., 62, 563–592, https://doi.org/10.1016/j.jhevol.2012.01.011, 2012.

Blumenthal, S. A.: Isotopic records of climate seasonality in equid teeth, Geochim. Cosmochim. Acta, 20, 2019.

Blumenthal, S. A., Levin, N. E., Brown, F. H., Brugal, J.-P., Chritz, K. L., Harris, J. M., Jehle, G. E., and Cerling, T. E.: Aridity and hominin environments, PNAS, 6, 2017.

Boucher, O., Denvil, S., Levavasseur, G., Cozic, A., Caubel, A., Foujols, M.-A., Meurdesoif, Y., Cadule, P., Devilliers, M., Ghattas, J., Lebas, N., Lurton, T., Mellul, L., Musat, I., Mignot, J., and Cheruy, F.: IPSL IPSL-CM6A-LR model output prepared for CMIP6 CMIP amip, , https://doi.org/10.22033/ESGF/CMIP6.5113, 2018.

Boucher, O., Servonnat, J., Albright, A. L., Aumont, O., Balkanski, Y., Bastrikov, V., Bekki, S., Bonnet, R., Bony, S., Bopp, L., Braconnot, P., Brockmann, P., Cadule, P., Caubel, A., Cheruy, F., Codron, F., Cozic, A., Cugnet, D., D’Andrea, F., Davini, P., Lavergne, C., Denvil, S., Deshayes, J., Devilliers, M., Ducharne, A., Dufresne, J., Dupont, E., Éthé, C., Fairhead, L., Falletti, L., Flavoni, S., Foujols, M., Gardoll, S., Gastineau, G., Ghattas, J., Grandpeix, J., Guenet, B., Guez, L., E., Guilyardi, E., Guimberteau, M., Hauglustaine, D., Hourdin, F., Idelkadi, A., Joussaume, S., Kageyama, M., Khodri, M., Krinner, G., Lebas, N., Levavasseur, G., Lévy, C., Li, L., Lott, F., Lurton, T., Luyssaert, S., Madec, G., Madeleine, J., Maignan, F., Marchand, M., Marti, O., Mellul, L., Meurdesoif, Y., Mignot, J., Musat, I., Ottlé, C., Peylin, P., Planton, Y., Polcher, J., Rio, C., Rochetin, N., Rousset, C., Sepulchre, P., Sima, A., Swingedouw, D., Thiéblemont, R., Traore, A. K., Vancoppenolle, M., Vial, J., Vialard, J., Viovy, N., and Vuichard, N.: Presentation and Evaluation of the IPSL-CM6A-LR Climate Model, J. Adv. Model. Earth Syst., 12, https://doi.org/10.1029/2019MS002010, 2020.

Braconnot, P., Harrison, S. P., Kageyama, M., Bartlein, P. J., Masson-Delmotte, V., Abe-Ouchi, A., Otto-Bliesner, B., and Zhao, Y.: Evaluation of climate models using palaeoclimatic data, Nat. Clim. Change, 417–424, 8, 2012.

Braconnot, P., Albani, S., Balkanski, Y., Cozic, A., Kageyama, M., Sima, A., Marti, O., and Peterschmitt, J.-Y.: Impact of dust in PMIP-CMIP6 mid-Holocene simulations with the IPSL model, Clim. Past, 17, 1091–1117, https://doi.org/10.5194/cp-17-1091-2021, 2021.

Carto, S. L., Weaver, A. J., Hetherington, R., Lam, Y., and Wiebe, E. C.: Out of Africa and into an ice age: on the role of global climate change in the late Pleistocene migration of early modern humans out of Africa, J. Hum. Evol., 56, 139–151, https://doi.org/10.1016/j.jhevol.2008.09.004, 2009.

Chapman, J. W., Klaassen, R. H. G., Drake, V. A., Fossette, S., Hays, G. C., Metcalfe, J. D., Reynolds, A. M., Reynolds, D. R., and Alerstam, T.: Animal Orientation Strategies for Movement in Flows, Curr. Biol., 21, R861–R870, https://doi.org/10.1016/j.cub.2011.08.014, 2011.

Comay, O. and Dayan, T.: From micromammals to paleoenvironments, Archaeol. Anthropol. Sci., 10, 2159–2171, https://doi.org/10.1007/s12520-018-0608-8, 2018.

Cornette, R., Stoetzel, E., Baylac, M., Moulin, S., Hutterer, R., Nespoulet, R., El Hajraoui, M. A., Denys, C., and Herrel, A.: Shrews of the genus Crocidura from El Harhoura 2 (Témara, Morocco): The contribution of broken specimens to the understanding of Late Pleistocene–Holocene palaeoenvironments in North Africa, Palaeogeogr. Palaeoclimatol. Palaeoecol., 436, 1–8, https://doi.org/10.1016/j.palaeo.2015.06.020, 2015.

Couvreur, T. L. P., Dauby, G., Blach-Overgaard, A., Deblauwe, V., Dessein, S., Droissart, V., Hardy, O. J., Harris, D. J., Janssens, S. B., Ley, A. C., Mackinder, B. A., Sonké, B., Sosef, M. S. M., Stévart, T., Svenning, J., Wieringa, J. J., Faye, A., Missoup, A. D., Tolley, K. A., Nicolas, V., Ntie, S., Fluteau, F., Robin, C., Guillocheau, F., Barboni, D., and Sepulchre, P.: Tectonics, climate and the diversification of the tropical African terrestrial flora and fauna, Biol. Rev., 96, 16–51, https://doi.org/10.1111/brv.12644, 2020.

deMenocal, P. B.: Plio-Pleistocene African Climate, Science, 270, 53–59, https://doi.org/10.1126/science.270.5233.53, 1995.

deMenocal, P. B.: African climate change and faunal evolution during the Pliocene–Pleistocene, Earth Planet. Sci. Lett., 220, 3–24, https://doi.org/10.1016/S0012-821X(04)00003-2, 2004.

Denys, C., Stoetzel, E., Andrews, P., Bailon, S., Rihane, A., Huchet, J. B., Fernandez-Jalvo, Y., and Laroulandie, V.: Taphonomy of Small Predators multi-taxa accumulations: palaeoecological implications, Hist. Biol., 30, 868–881, https://doi.org/10.1080/08912963.2017.1347647, 2018.

Drake, N. A., Blench, R. M., Armitage, S. J., Bristow, C. S., and White, K. H.: Ancient watercourses and biogeography of the Sahara explain the peopling of the desert, Proc. Natl. Acad. Sci., 108, 458–462, https://doi.org/10.1073/pnas.1012231108, 2011.

Drake, N. A., Breeze, P., and Parker, A.: Palaeoclimate in the Saharan and Arabian Deserts during the Middle Palaeolithic and the potential for hominin dispersals, Quat. Int., 300, 48–61, https://doi.org/10.1016/j.quaint.2012.12.018, 2013.

Dufresne, J.-L., Foujols, M.-A., Denvil, S., Caubel, A., Marti, O., Aumont, O., Balkanski, Y., Bekki, S., Bellenger, H., Benshila, R., Bony, S., Bopp, L., Braconnot, P., Brockmann, P., Cadule, P., Cheruy, F., Codron, F., Cozic, A., Cugnet, D., de Noblet, N., Duvel, J.-P., Ethé, C., Fairhead, L., Fichefet, T., Flavoni, S., Friedlingstein, P., Grandpeix, J.-Y., Guez, L., Guilyardi, E., Hauglustaine, D., Hourdin, F., Idelkadi, A., Ghattas, J., Joussaume, S., Kageyama, M., Krinner, G., Labetoulle, S., Lahellec, A., Lefebvre, M.-P., Lefevre, F., Levy, C., Li, Z. X., Lloyd, J., Lott, F., Madec, G., Mancip, M., Marchand, M., Masson, S., Meurdesoif, Y., Mignot, J., Musat, I., Parouty, S., Polcher, J., Rio, C., Schulz, M., Swingedouw, D., Szopa, S., Talandier, C., Terray, P., Viovy, N., and Vuichard, N.: Climate change projections using the IPSL-CM5 Earth System Model: from CMIP3 to CMIP5, Clim. Dyn., 40, 2123–2165, https://doi.org/10.1007/s00382-012-1636-1, 2013.

Duplessy, J.-C. and Ramstein, G.: Paléonclimatologie, tome II : enquêter sur les climats anciens., CNRS Editions., 2013.

Ebrahimi-Khusfi, Z., Mirakbari, M., and Khosroshahi, M.: Vegetation response to changes in temperature, rainfall, and dust in arid environments, Environ. Monit. Assess., 192, 691, https://doi.org/10.1007/s10661-020-08644-0, 2020.

Eyring, V., Bony, S., Meehl, G. A., Senior, C. A., Stevens, B., Stouffer, R. J., and Taylor, K. E.: Overview of the Coupled Model Intercomparison Project Phase 6 (CMIP6) experimental design and organization, Geosci. Model Dev., 9, 1937–1958, https://doi.org/10.5194/gmd-9-1937-2016, 2016.

Fernandez-Jalvo, Y., Denys, C., Andrews, P., Williams, T., Dauphin, Y., and Humphrey, L.: Taphonomy and palaeoecology of Olduvai Bed-I (Pleistocene, Tanzania), J. Hum. Evol., 34, 137–172, 1998.

Fyllas, N. M., Bentley, L. P., Shenkin, A., Asner, G. P., Atkin, O. K., Díaz, S., Enquist, B. J., Farfan-Rios, W., Gloor, E., Guerrieri, R., Huasco, W. H., Ishida, Y., Martin, R. E., Meir, P., Phillips, O., Salinas, N., Silman, M., Weerasinghe, L. K., Zaragoza-Castells, J., and Malhi, Y.: Solar radiation and functional traits explain the decline of forest primary productivity along a tropical elevation gradient, Ecol. Lett., 20, 730–740, https://doi.org/10.1111/ele.12771, 2017.

Ghawar, W., Zaätour, W., Chlif, S., Bettaieb, J., Chelghaf, B., Snoussi, M.-A., and Salah, A. B.: Spatiotemporal dispersal of Meriones shawi estimated by radio-telemetry, Int. J. Multidiscip. Res. Dev., 2, 211–216, 2015.

Gillooly, J. F., Brown, J. H., West, G. B., Savage, V. M., and Charnov, E. L.: Effects of Size and Temperature on Metabolic Rate, Science, 293, 2248–2251, 2001.

Hanon, R., Patou-Mathis, M., Péan, S., and Prat, S.: Paleobiodiversity and large mammal associations during the late Pliocene and the Early Pleistocene in South Africa, Quaternaire, 243–256, https://doi.org/10.4000/quaternaire.12131, 2019.

Harrison, S. P., Bartlein, P. J., Izumi, K., Li, G., Annan, J., Hargreaves, J., Braconnot, P., and Kageyama, M.: Evaluation of CMIP5 palaeo-simulations to improve climate projections, Nat.

Clim. Change, 5, 735–743, https://doi.org/10.1038/nclimate2649, 2015.

Haywood, A. M., Dowsett, H. J., Dolan, A. M., Rowley, D., Abe-Ouchi, A., Otto-Bliesner, B., Chandler, M. A., Hunter, S. J., Lunt, D. J., Pound, M., and Salzmann, U.: The Pliocene Model Intercomparison Project (PlioMIP) Phase 2: scientific objectives and experimental design, Clim. Past, 12, 663–675, https://doi.org/10.5194/cp-12-663-2016, 2016.

Hijmans, R. J. and van Etten, J.: raster: Geographic analysis and modeling with raster data. R package version 2.0-12., 2012.

Hooghiemstra, H., Stalling, H., Agwu, C. O. C., and Dupont, L. M.: Vegetational and climatic changes at the northern fringe of the sahara 250,000–5000 years BP: evidence from 4 marine pollen records located between Portugal and the Canary Islands, Rev. Palaeobot. Palynol., 74, 1–53, https://doi.org/10.1016/0034-6667(92)90137-6, 1992.

Hourdin, F., Rio, C., Grandpeix, J., Madeleine, J., Cheruy, F., Rochetin, N., Jam, A., Musat, I., Idelkadi, A., Fairhead, L., Foujols, M., Mellul, L., Traore, A., Dufresne, J., Boucher, O., Lefebvre, M., Millour, E., Vignon, E., Jouhaud, J., Diallo, F. B., Lott, F., Gastineau, G., Caubel, A., Meurdesoif, Y., and Ghattas, J.: LMDZ6A: The Atmospheric Component of the IPSL Climate Model With Improved and Better Tuned Physics, J. Adv. Model. Earth Syst., 12, https://doi.org/10.1029/2019MS001892, 2020.

Hovenden, M. J., Vander Schoor, J. K., and Osanai, Y.: Relative humidity has dramatic impacts on leaf morphology but little effect on stomatal index or density in Nothofagus cunninghamii (Nothofagaceae), Aust. J. Bot., 60, 700, https://doi.org/10.1071/BT12110, 2012.

Jacobs, Z., Roberts, R. G., Nespoulet, R., El Hajraoui, M. A., and Debénath, A.: Single-grain OSL chronologies for Middle Palaeolithic deposits at El Mnasra and El Harhoura 2, Morocco: Implications for Late Pleistocene human–environment interactions along the Atlantic coast of northwest Africa, J. Hum. Evol., 62, 377–394, https://doi.org/10.1016/j.jhevol.2011.12.001, 2012.

Janati-Idrissi, N., Falgueres, C., Nespoulet, R., El Hajraoui, M. A., Debénath, A., Bejjit, L., Bahain, J.-J., Michel, P., Garcia, T., Boudad, L., El Hammouti, K., and Oujaa, A.: Datation par ESR-U/th combinées de dents fossiles des grottes d'El Mnasra et d'El Harhoura 2, région de Rabat-Temara. Implications chronologiques sur le peuplement du Maroc atlantique au Pléistocène supérieur et son, Quaternaire, 23, 25–35, https://doi.org/10.4000/quaternaire.6127, 2012.

Jeffrey, A.: Exploring palaeoaridity using stable oxygen and carbon isotopes in small mammal teeth: a case study from two Late Pleistocene archaeological cave sites in Morocco, North Africa, 2016.

Jolliffe, I. T. and Cadima, J.: Principal component analysis: a review and recent developments, Philos. Trans. R. Soc. Math. Phys. Eng. Sci., 374, 20150202, https://doi.org/10.1098/rsta.2015.0202, 2016.

Joussaume, S. and Braconnot, P.: Sensitivity of paleoclimate simulation results to season definitions, J. Geophys. Res. Atmospheres, 102, 1943–1956, https://doi.org/10.1029/96JD01989, 1997.

Kageyama, M., Braconnot, P., Bopp, L., Caubel, A., Foujols, M.-A., Guilyardi, E., Khodri, M., Lloyd, J., Lombard, F., Mariotti, V., Marti, O., Roy, T., and Woillez, M.-N.: Mid-Holocene and Last Glacial Maximum climate simulations with the IPSL model—part I: comparing IPSL_CM5A to IPSL_CM4, Clim. Dyn., 40, 2447–2468, https://doi.org/10.1007/s00382-012-1488-8, 2013.

Kageyama, M., Braconnot, P., Harrison, S. P., Haywood, A. M., Jungclaus, J. H., Otto-Bliesner, B. L., Peterschmitt, J.-Y., Abe-Ouchi, A., Albani, S., Bartlein, P. J., Brierley, C., Crucifix, M., Dolan, A., Fernandez-Donado, L., Fischer, H., Hopcroft, P. O., Ivanovic, R. F., Lambert, F., Lunt, D. J., Mahowald, N. M., Peltier, W. R., Phipps, S. J., Roche, D. M., Schmidt, G. A., Tarasov, L., Valdes, P. J., Zhang, Q., and Zhou, T.: The PMIP4 contribution to CMIP6 – Part 1: Overview and over-arching analysis plan, Geosci. Model Dev., 11, 1033–1057, https://doi.org/10.5194/gmd-11-1033-2018, 2018.

Kassambara, A. and Mundt, F.: Factoextra: Extract and Visualize the Results of Multivariate Data Analyses. R Package Version 1.0.7., 2020.

Kutzbach, J. E. and Otto-Bliesner, B. L.: The Sensitivity of the African-Asian Monsoonal Climate to Orbital Parameter Changes for 9000 Years B.P. in a Low-Resolution General Circulation Model, J. Atmospheric Sci., 39, 1982.

Le Houérou, H. N.: Climate, flora and fauna changes in the Sahara over the past 500 million years, J. Arid Environ., 37, 619–647, https://doi.org/10.1006/jare.1997.0315, 1997.

Lê, S., Josse, J., and Husson, F.: FactoMineR: an R Package for multivariate analysis, J. Stat. Softw., 25, https://doi.org/10.18637/jss.v025.i01, 2008.

Lin, G.: Chapter 4: Research on stable isotope and carbon cycle (1st ed.), in: Stable Isotope Ecology, Beijing, 89–123, 2013.

Lionello, P., Malanotte, P., and Boscolo, R. (Eds.): Mediterranean Climate Variability, Elsevier., Elsevier, Amsterdam, 2006.

Longinelli, A. and Selmo, E.: Isotopic composition of precipitation in Italy: a first overall map, J. Hydrol., 270, 75–88, https://doi.org/10.1016/S0022-1694(02)00281-0, 2003.

Marquer, L., Otto, T., Ben Arous, E., Stoetzel, E., Campmas, E., Zazzo, A., Tombret, O., Falgueres, C., El Hajraoui, M. A., and Nespoulet, R.: The first use of olives in Africa around 100,000 years ago, Nat. Plants, 8, 204–208, 2022.

Marti, O., Braconnot, P., Dufresne, J.-L., Bellier, J., Benshila, R., Bony, S., Brockmann, P., Cadule, P., Caubel, A., Codron, F., de Noblet, N., Denvil, S., Fairhead, L., Fichefet, T., Foujols, M.-A., Friedlingstein, P., Goosse, H., Grandpeix, J.-Y., Guilyardi, E., Hourdin, F., Idelkadi, A., Kageyama, M., Krinner, G., Lévy, C., Madec, G., Mignot, J., Musat, I., Swingedouw, D., and Talandier, C.: Key features of the IPSL ocean atmosphere model and its sensitivity to atmospheric resolution, Clim. Dyn., 34, 1–26, https://doi.org/10.1007/s00382-009-0640-6, 2010.

Martínez-Blancas, A. and Martorell, C.: Changes in niche differentiation and environmental filtering over a hydric stress gradient, J. Plant Ecol., 13, 185–194, https://doi.org/10.1093/jpe/rtz061, 2020.

Matthews, T.: Predators, prey and the palaeoenvironment., South Afr. J. Sci., 95, 22–24, 2000.

McNeil, J. N.: Behavioral Ecology of Pheromone-Mediated Communication in Moths and Its Importance in the Use of Pheromone Traps, Annu. Rev. Enthomology, 36, 407–30, 1991.

Michel, P., Campmas, É., Stoetzel, E., Nespoulet, R., Abdeljalil El Hajraoui, M., and Amani, F.: La macrofaune du Pléistocène supérieur d’El Harhoura 2 (Témara, Maroc) : données préliminaires, L’Anthropologie, 113, 283–312, https://doi.org/10.1016/j.anthro.2009.04.003, 2009.

Monteith, J. L.: Solar Radiation and Productivity in Tropical Ecosystems, J. Appl. Ecol., 9, 747, https://doi.org/10.2307/2401901, 1972.

Navarro, N., Lécuyer, C., Montuire, S., Langlois, C., and Martineau, F.: Oxygen isotope compositions of phosphate from arvicoline teeth and Quaternary climatic changes, Gigny, French Jura, Quat. Res., 62, 172–182, https://doi.org/10.1016/j.yqres.2004.06.001, 2004.

Nespoulet, R. and El Hajraoui, M. A.: Excavation report, 2012.

Neuwirth, E.: RColorBrewer: ColorBrewer palettes. R package version 1.1-2., 2014.

O'Leary, M. H.: Carbon Isotopes in Photosynthesis, BioScience, 38, 328–336, https://doi.org/10.2307/1310735, 1988.

Otto-Bliesner, B. L., Brady, E. C., Zhao, A., Brierley, C. M., Axford, Y., Capron, E., Govin, A., Hoffman, J. S., Isaacs, E., Kageyama, M., Scussolini, P., Tzedakis, P. C., Williams, C. J. R., Wolff, E., Abe-Ouchi, A., Braconnot, P., Ramos Buarque, S., Cao, J., de Vernal, A., Guarino, M. V., Guo, C., LeGrande, A. N., Lohmann, G., Meissner, K. J., Menviel, L., Morozova, P. A., Nisancioglu, K. H., O'ishi, R., Salas y Mélia, D., Shi, X., Sicard, M., Sime, L., Stepanek, C., Tomas, R., Volodin, E., Yeung, N. K. H., Zhang, Q., Zhang, Z., and Zheng, W.: Large-scale features of Last Interglacial climate: results from evaluating the <i>lig127k<i/> simulations for the Coupled Model Intercomparison Project (CMIP6)–Paleoclimate Modeling Intercomparison Project (PMIP4), Clim. Past, 17, 63–94, https://doi.org/10.5194/cp-17-63-2021, 2021.

Paz, H., Pineda-García, F., and Pinzón-Pérez, L. F.: Root depth and morphology in response to soil drought: comparing ecological groups along the secondary succession in a tropical dry forest, Oecologia, 179, 551–561, https://doi.org/10.1007/s00442-015-3359-6, 2015.

Pebesma, E. and Bivand, R.: S Classes and Methods for Spatial Data: the sp Package, 2005.

Pellegrino, A. C., Peñaflor, M. F. G. V., Nardi, C., Bezner-Kerr, W., Guglielmo, C. G., Bento, J. M. S., and McNeil, J. N.: Weather Forecasting by Insects: Modified Sexual Behaviour in Response to Atmospheric Pressure Changes, PLoS ONE, 8, e75004, https://doi.org/10.1371/journal.pone.0075004, 2013.

Pickering, R., Herries, A. I. R., Woodhead, J. D., Hellstrom, J. C., Green, H. E., Paul, B., Ritzman, T., Strait, D. S., Schoville, B. J., and Hancox, P. J.: U–Pb-dated flowstones restrict South African early hominin record to dry climate phases, Nature, 565, 226–229, https://doi.org/10.1038/s41586-018-0711-0, 2019.

R Development Core Team: R: A language and environment for statistical computing. R Foundation for Statistical Computing, Vienna, Austria. ISBN 3-900051-07-0, URL: http://www.R-project.org., 2018.

Royer, A., Lécuyer, C., Montuire, S., Amiot, R., Legendre, S., Cuenca-Bescós, G., Jeannet, M., and Martineau, F.: What does the oxygen isotope composition of rodent teeth record?, Earth Planet. Sci. Lett., 361, 258–271, https://doi.org/10.1016/j.epsl.2012.09.058, 2013.

Sampson, P. D., Streissguth, A. P., and Bookstein, F. L.: Neurobehavioral Effects of Prenatal Alcohol: Part II. Partial Least Squares Analysis I, Neurotoxicol. Teratol., 11, 477–491, 1989.

Schmidt, G. A., Annan, J. D., Bartlein, P. J., Cook, B. I., Guilyardi, E., Hargreaves, J. C., Harrison, S. P., Kageyama, M., LeGrande, A. N., Konecky, B., Lovejoy, S., Mann, M. E., Masson-Delmotte, V., Risi, C., Thompson, D., Timmermann, A., Tremblay, L.-B., and Yiou, P.: Using palaeo-climate comparisons to constrain future projections in CMIP5, Clim. Past, 10, 221–250, https://doi.org/10.5194/cp-10-221-2014, 2014.

Schulzweida, U.: CDO User Guide (Version 1.9.8), 2019.

Sicard, M., Kageyama, M., Charbit, S., Braconnot, P., and Madeleine, J.-B.: An energy budget approach to understand the Arctic warming during the Last Interglacial, Clim. Past, 18, 607–629, https://doi.org/10.5194/cp-18-607-2022, 2022.

Smiley, T. M., Cotton, J. M., Badgley, C., and Cerling, T. E.: Small-mammal isotope ecology tracks climate and vegetation gradients across western North America, Oikos, 125, 1100–1109, https://doi.org/10.1111/oik.02722, 2016.

Sobrino, J. A. and Raissouni, N.: Toward remote sensing methods for land cover dynamic monitoring: Application to Morocco, Int. J. Remote Sens., 21, 353–366, https://doi.org/10.1080/014311600210876, 2000.

Stoetzel, E.: Les microvertébrés du site d'occupation humaine d'El Harhoura 2 (Pleistocene supérieur - Holocène, Maroc) : systématique, évolution, taphonomie et paléoécologie., 437, 2009.

Stoetzel, E., Marion, L., Nespoulet, R., El Hajraoui, M. A., and Denys, C.: Taphonomy and palaeoecology of the late Pleistocene to middle Holocene small mammal succession of El Harhoura 2 cave (Rabat-Témara, Morocco), J. Hum. Evol., 60, 1–33, https://doi.org/10.1016/j.jhevol.2010.07.016, 2011.

Stoetzel, E., Bougariane, B., Campmas, E., Ouchaou, B., and Michel, P.: Chapitre V. Faunes et paléoenvironnements., in: Préhistoire de la région de Rabat-Témara., vol. 3, Rabat, 35–51, 2012a.

Stoetzel, E., Denys, C., Bailon, S., El Hajraoui, M. A., and Nespoulet, R.: Taphonomic Analysis of Amphibian and Squamate Remains from El Harhoura 2 (Rabat-Témara, Morocco): Contributions to Palaeoecological and Archaeological Interpretations: Taphonomic Study of Amphibian and Squamate Fossil Remains, Int. J. Osteoarchaeol., 22, 616–635, https://doi.org/10.1002/oa.1275, 2012b.

Stoetzel, E., Campmas, E., Michel, P., Bougariane, B., Ouchaou, B., Amani, F., El Hajraoui, M. A., and Nespoulet, R.: Context of modern human occupations in North Africa: Contribution of the Témara caves data, Quat. Int., 320, 143–161, https://doi.org/10.1016/j.quaint.2013.05.017, 2014.

Stoetzel, E., Lalis, A., Nicolas, V., Aulagnier, S., Benazzou, T., Dauphin, Y., El Hajraoui, M. A., El Hassani, A., Fahd, S., Fekhaoui, M., Geigl, E.-M., Lapointe, F.-J., Leblois, R., Ohler, A., Nespoulet, R., and Denys, C.: Quaternary terrestrial microvertebrates from mediterranean northwestern Africa: State-of-the-art focused on recent multidisciplinary studies, Quat. Sci. Rev., 224, 105966, https://doi.org/10.1016/j.quascirev.2019.105966, 2019.

Streissguth, A. P., Bookstein, F. L., Sampson, P. D., and Barr, H. M.: The enduring effects of prenatal alcohol exposure on child development: Birth through seven years, a partial least squares solution., The University of Michigan Press., 1993.

Tanner, E. V. J., Kapos, V., and Healey, J. R.: Hurricane Effects on Forest Ecosystems in the Caribbean, Biotropica, 23, 513, https://doi.org/10.2307/2388274, 1991.

Tieszen, L. L.: Natural variations in the carbon isotope values of plants: Implications for archaeology, ecology, and paleoecology, J. Archaeol. Sci., 18, 227–248, https://doi.org/10.1016/0305-4403(91)90063-U, 1991.

Trauth, M. H., Larrasoaña, J. C., and Mudelsee, M.: Trends, rhythms and events in Plio-Pleistocene African climate, Quat. Sci. Rev., 28, 399–411, https://doi.org/10.1016/j.quascirev.2008.11.003, 2009.

Warnes, G., Bolker, B., Gorjanc, G., Grothendieck, G., Korosec, A., Lumley, T., MacQueen, D., Magnusson, A., and Rogers, J.: gdata: Various R programming tools for data manipulation, 2005.

Wei, T. and Simko, V.: R package “corrplot”: Visualization of a Correlation Matrix. (Version 0.90), 2021.

Wickham, H.: ggplot2: elegant graphics for data analysis., Springer, 2015.

Yom-Tov, Y. and Geffen, E.: Geographic variation in body size: the effects of ambient temperature and precipitation, Oecologia, 148, 213–218, https://doi.org/10.1007/s00442-006-0364-9, 2006.